Applied Energy

Achieving high-efficiency conversion and poly-generation of cooling, heating, and power based on biomass-fueled SOFC hybrid system: Performance assessment and multi-objective optimization

--Manuscript Draft--

Manuscript Number:	
Article Type:	Research Paper
Keywords:	Biomass energy, SOFC hybrid system, Thermodynamic analysis, Multi-objective optimization
Corresponding Author:	Zhen Wu, Ph.D. Xi'an Jiaotong University Xi'an, CHINA
First Author:	Pengfei Zhu
Order of Authors:	Pengfei Zhu
	Jing Yao
	Leilei Guo
	Min Dai
	Jianwei Ren, Ph.D
	Sandra Kurko, Ph.D
	Zhen Wu, Ph.D.
	Fusheng Yang, Ph.D
	Zaoxiao Zhang, Ph.D
Abstract:	In order to develop clean and efficient energy conversion technology, a novel combined cooling, heating and power (CCHP) system using biomass as fuel is proposed in this work. The proposed CCHP system consists of biomass gasification unit, solid oxide fuel cell (SOFC) and engine power generation unit and absorption refrigeration unit. Thermodynamic model of the CCHP system is developed for the parametric and exergy analyses to evaluate the performance. The parametric analysis shows that increasing the steam to biomass ratio or the SOFC fuel utilization factor helps to improve the electrical efficiency, while the increase of air equivalent ratio has a negative effect. The exergy analysis shows that the two units of biomass gasification and engine power generation have the largest exergy destruction ratio, which is 46.9% and 16.8% under the biomass flux of 500 kg·h $^{-1}$. This is because these two units involve in high-temperature thermochemical reaction process, resulting in relatively large exergy destruction. Besides, the tradeoff between maximum exergy efficiency, CCHP efficiency and minimum total annual cost is conducted by multi-objective optimization. Through optimization, the system could reach the high CCHP efficiency of 75 % and net electrical efficiency of 52%, as well as the low total annual cost of 410 k$ simultaneously. This work could provide the basic design idea, and high-efficiency and low-cost operation strategy for the practical application of the proposed novel biomass-fueled CCHP poly-generation system.
Suggested Reviewers:	Meng Ni, Ph.D Professor, The Hong Kong Polytechnic University meng.ni@polyu.edu.hk Prof. Meng Ni is an expert in the SOFC-based energy system.
	Jiri J. Klemes, Ph.D Professor, Pázmány Péter Catholic University klemes.jiri@itk.ppku.hu Prof. Klemes is an expert in the renewable energy system.
	Yingru Zhao, Ph.D Professor, Xiamen University

	yrzhao@xmu.edu.cn Prof. Yingru Zhao is an expert in energy system modeling and optimization.

Highlights

- Achieving efficient conversion from biomass to thermal, electric and cooling energy.
- The CCHP system has high electrical efficiency of 52% and overall efficiency of 75%.
- The 3E evaluations and multi-objective optimization are conducted.
- Equations between efficiency and cost are fitted for efficient and economic operation strategy.

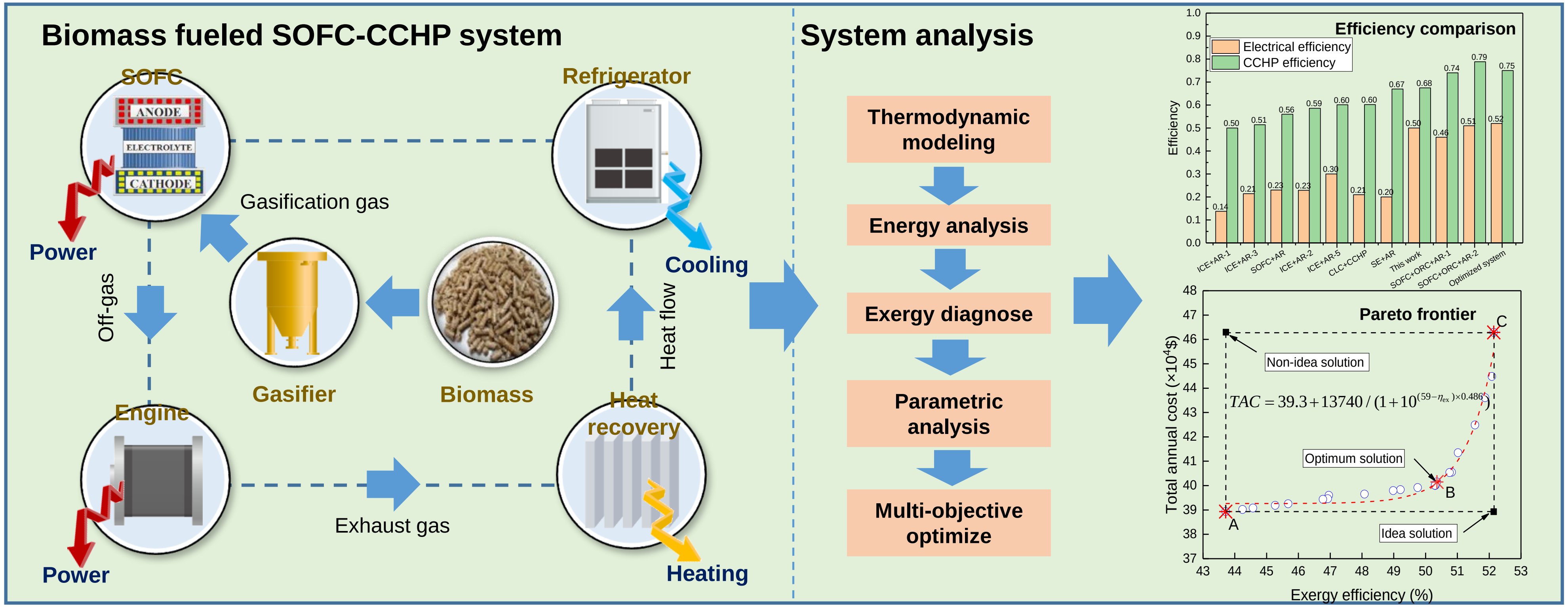

Biomass fueled SOFC-CCHP system
SOFC
ANODE
ELECTROLYTE
CATHODE
Refrigerator
Gasification gas
Power
Cooling
Off-gas
Gasifier
Biomass
Heat flow
Engine
Heat recovery
Exhaust gas
Power
Heating
System analysis
Thermodynamic modeling
Energy analysis
Exergy diagnose
Parametric analysis
Multi-objective optimize
Efficiency comparison
Electrical efficiency
CCHP efficiency
Efficiency
ICE+AR-1
ICE+AR-3
SOFC+AR
ICE+AR-2
ICE+AR-5
CLC+CCHP
SE+AR
This work
SOFC+ORC+AR-1
SOFC+ORC+AR-2
Optimized system
Pareto frontier
Non-idea solution
$TAC = 39.3 + 13740 / (1 + 10^{(59-\eta_{ex}) \times 0.486})$
Optimum solution
Idea solution
A
B
C
Total annual cost (×10^4\$)
Exergy efficiency (%)

Achieving high-efficiency conversion and poly-generation of cooling, heating, and power based on biomass-fueled SOFC hybrid system: Performance assessment and multi-objective optimization

Pengfei Zhu[1], Jing Yao[1], Leilei Guo[1], Min Dai[1], Jianwei Ren[2], Sandra Kurko[3], Zhen Wu[1*], Fusheng Yang[1], Zaoxiao Zhang[1,4]

1 School of Chemical Engineering and Technology, Xi'an Jiaotong University, Xi'an, 710049, China

2 Department of Mechanical Engineering Science, University of Johannesburg, Johannesburg, 2092, South Africa

3 Center of Excellence for Hydrogen and Renewable Energy, Vinča Institute of Nuclear Sciences, University of Belgrade, 11351, Belgrade, Serbia

4 State Key Laboratory of Multiphase Flow for Power Engineering, Xi'an Jiaotong University, Xi'an, 710049, China

Corresponding Author, wuz2015@xjtu.edu.cn (Z. Wu)

Abstract

In order to develop clean and efficient energy conversion technology, a novel combined cooling, heating and power (CCHP) system using biomass as fuel is proposed in this work. The proposed CCHP system consists of biomass gasification unit, solid oxide fuel cell (SOFC) and engine power generation unit and absorption refrigeration unit. Thermodynamic model of the CCHP system is developed for the parametric and exergy analyses to evaluate the performance. The parametric analysis shows that increasing the steam to biomass ratio or the SOFC fuel utilization factor helps to improve the electrical efficiency, while the increase of air equivalent ratio has a negative effect. The exergy analysis shows that the two units of biomass gasification and engine power generation have the largest exergy destruction ratio, which is 46.9% and 16.8% under the biomass flux of 500 kg·h^{-1}. This is because these two units involve in high-temperature thermochemical reaction process, resulting in relatively large exergy destruction. Besides, the tradeoff between maximum exergy efficiency, CCHP efficiency and minimum total annual cost is conducted by multi-objective optimization. Through optimization, the system could reach the high CCHP efficiency of 75 % and net electrical efficiency of 52%, as well as the low total annual cost of 410 k$ simultaneously. This work could provide the basic design idea, and high-efficiency and low-cost operation strategy for the practical application of the proposed novel biomass-fueled CCHP poly-generation system.

Keywords: Biomass energy, SOFC hybrid system, Thermodynamic analysis, Multi-objective optimization.

Nomenclature

Abbreviation		*Greek*	
AB	Air blower	α	Biomass conversion ratio
AR	Absorption refrigeration	β	Multiplication factor
CCHP	Combined cooling heating and power	γ	Compression ratio
ED	Euclidian distance	ΔH	Reaction enthalpy
ER	Air equivalent ratio	ε	Polytropic index
FC	Fuel cell	η	Efficiency
HCCI	Homogeneous charge compression ignition	λ	Expansion ratio
HEX	Heat exchanger	μ	Fuel utilization factor
LHV	Lower heating value		
MSR	Methane steam reforming	*Subscripts and superscripts*	
PER	Primary energy rate	act	Activation overvoltage
PESR	Primary energy saving ratio	bio	Biomass
S/B	Steam to biomass ratio	C	Cooling or compression process
SOFC	Solid oxide fuel cell	ch	Chemical
TAC	Total annual cost	conc	Concentration overvoltage
WGS	Water gas shift	D	Destruction
WHC	Waste heat collector	E	Expansion process or electricity
		ex	Exergy
Symbols		F	Fuel
Ac	Area of single cell, m^2	G	Gross
C	Capital cost, $	H	Heating
E	Electromotive force, V	I	Inverter or independent production
$\dot{E}x$	Exergy flow, kW	in	Inlet
$\dot{e}x$	Specific exergy, kJ/mol	ME	Mechanical efficiency for expansion
F	Faraday constant, C/mol	MEC	Mechanical efficiency for compression
h	Specific enthalpy, kJ/mol	N	Net
J	Current density, A/m^2	ohm	Ohm overvoltage
$\dot{m}$	Mass flow, kg/h	out	outlet
N	Number of single cell	P	Pump or Product
n	Number of transferred electrons	ph	Physical
p	Pressure or partial pressure, bar	POC	Polytropic efficiency for compression
$\dot{Q}$	Thermal power, kW	POE	Polytropic efficiency for expansion
R	Ideal gas constant, J/(mol·K)	re	Reversible
s	Specific entropy, kJ/(mol·K)	0	Environmental state
T	Temperature, ^{o}C		
V	Fuel cell output voltage, V		
$\dot{W}$	Power, kW		
x	Mass fraction		
y	Exergy destruction ratio		

1. Introduction

Traditional energy systems based on fossil fuels are the main way of generating electricity and contribute to the most of the worldwide energy demand. However, the overuse of fossil fuels has also brought about the severe threat of global environmental degradation and energy shortages [1]. At the same time, the fossil fuels consumption runs counter to the concept of sustainable development. In order to alleviate the contradiction between increasing energy demand and social development in a sustainable and environmentally friendly way, clean and efficient energy conversion technologies have been developed greatly in the past few years [2]. In such framework, the utilization and development of renewable energy gradually become one of the main research directions at present [3]. Among all the renewable energy sources, biomass energy is the fourth largest energy source in the world, accounting for nearly 14% of the world's primary energy demand [4]. Therefore, the clean and efficient utilization of biomass energy has become an important issue in the field of renewable energy.

Fuel cell (FC) is known as the next power generation technology due to its excellent energy conversion performance and free-pollution. The FC enables to achieve high energy conversion efficiency, because it is not limited by Carnot cycle [5]. In addition, no high temperature combustion process occurs so that no nitrogen and sulfur oxides emissions appear, which helps to the environmental protection [6]. As a kind of high-temperature fuel cell, solid oxide fuel cell (SOFC) usually operates at the temperature around 800 ^{o}C, indicating that it is flexible for SOFC to using hydrocarbon fuel, because the fuel can be pretreated by reforming and shifting reactions at high temperatures. The gasification, as one of the main utilization methods of biomass, can produce syngas with hydrogen, oxygen and low carbon hydrocarbons under the action of gasifying agent [7]. Therefore, the integration of biomass gasification and SOFC is expected to achieve the target of clean and efficient energy conversion.

Not surprisingly, the biomass based SOFC hybrid systems have also been investigated by many scholars from model and experiment perspectives. Radenahmad et al. [8] overviewed the SOFC system for heating and power production driven by biomass gasification and discussed the present status and future prospect of this technology. It was recommended that by developing new anode material, the problem of SOFC carbon deposition can be better solved, thus enabling the hybrid system operate more stable. Yuksel et al. [9] designed a hybrid plant including a biomass gasifier, SOFC, ejector cooling and proton exchanger membrane electrolyzer to produce electricity, hydrogen, fresh and hot water, heating, and cooling. The thermodynamic evaluation results showed the energy and exergy efficiency of the whole system are 56.17% and 52.83%, respectively. An experimental study of the SOFC combined with gasification power plant concept was carried out by Gadsbøll et al. [10]. They reported that the biomass-to-electricity efficiencies is up to 43%. A steady-state model of a biomass-SOFC was developed using process simulation software, Aspen Plus, to predict performance under diverse operating conditions by Marcantonio et al. [11]. The low steam to biomass ratio is also preferably adopted and the electrical efficiency of the system under the operating conditions can reach 57%. Hosseinpour et al. [12] designed a biomass gasification integrated internal reforming SOFC plant, which is fueled by municipal solid waste. The hybrid system performance using four different gasification agents was compared from the points of energy, exergy, environmental and exergoeconomic analyses. The comparison results showed that the comprehensive performance of the system using oxygen as gasification agent is preferable, whose total exergy unit cost of products and CO_2 emission rate are 3.02 cent/kWh and 0.383 kg/kWh, respectively.

The above literature survey indicates that the SOFC hybrid plant integrated with biomass gasification has certain technological, economic and environmental advantages. Therefore, this kind of system is worthy of development and promotion. However, it should be noted that the off-gas of SOFC generally carries a large amount of thermal energy due to its high operating temperature. Besides, the electrochemical reaction in SOFC is not complete. Some unconsumed fuels with a certain chemical energy still leave in the off gas [13]. From this point view, the full utilization of energy carried by SOFC off-gas is an important approach to further improve the energy conversion efficiency of the fuel cell hybrid system [14]. Combining the SOFC-based system with other cycles or devices for energy recovery is one of the promising approaches. In our previous reports, it was confirmed that adopting engine as the SOFC downstream unit for secondary power generation significantly improves the system performance [15,16]. In addition, the SOFC based biomass gasification systems are generally oriented towards distributed generation scenarios due to due to flexibility of installation and wide availability of fuel source. As a distributed energy supply system, thermal and cooling energy are also indispensable energy supply forms besides electricity. Fortunately, the thermal energy from the SOFC exhaust can also drive the refrigerating subsystem to provide a certain amount of cold energy, which achieves the poly-generation system of combined cooling, heating and power (CCHP) and improves the comprehensive energy efficiency.

Mehr et al. [17] studied the feasibility of SOFC based CCHP system in wastewater treatment plants through thermodynamic assessment. Based on the simulation results, the electricity coverage of the proposed system can be increased by 27% and the 20 kW of cooling power in summer can be obtained. Zhao and Hou [18] established an SOFC and humid air turbine CCHP system based on solar methanol reforming under Aspen Plus environment. The calculation results showed that the total power efficiency, exergy efficiency and thermal efficiency are 57.2%, 63.0% and 87.1%, respectively. Mehrpooya et al. [19] conducted a technical performance analysis to the SOFC-based CCHP system which is supposed to being utilized to an educational building (900 m^2) in Iran. The net electrical efficiency of the SOFC with the power capacity of 120 kW is about 45% and the CCHP efficiency is nearly 60%. Meanwhile, the corresponding economic analysis gave an estimation of capital recovery period of 8.3 years. Jing et al. [20] established an SOFC-based CCHP system design and operation optimization model using mixed integer nonlinear programming theory. The proposed model is applied to a case study of a hospital in Shanghai (China), considering technical specifications, energy pricing and emission factors. The research results exhibit the environmental and economic merits of the SOFC-based CCHP system. Moussawi et al. [21] developed an environmentally friendly CCHP system based on SOFC for domestic applications. This system is evaluated under energy, exergy, economy, and environment (4E) analyses and optimized by multi-objective method. In addition, the off-grid following electrical load and on-grid base load operations strategies are adopted. The research results demonstrate that the system exhibits superior energy and economic performance under both strategies.

Based on the above analyses, a novel biomass based SOFC-Engine system for cooling, heating and power production was proposed in this work. The main starting point of the system design includes realizing the cascade utilization of energy, improving the energy utilization efficiency, and meeting customers' demand for distributed energy system. The thermodynamic model of the system is established first. Then the energy conversion performance and exergy dissipation of the proposed hybrid system are deeply investigated based on the parametric analysis. Finally, the multi-objective optimization is carried out to achieve the tradeoff between high-efficiency and low-cost of the CCHP poly-generation hybrid system.

The contribution of this article could be summarized as follows: (I) In terms of system configuration, the homogeneous charge compression ignition (HCCI) engine is used to generate additional power by utilizing the unconsumed SOFC off-gas fuels. Compared with the traditional configuration of recycling exhaust energy with the gas turbine, the power capacity of this kind of engine is more matching and the system is more stable under harsh working environment [16]. Moreover, absorption refrigeration cycle is adopted for cooling supply, which meets the diversified energy demand. (II) The system was modeled by the chemical process simulation software Aspen Plus©, and the basic thermodynamic data of the system operation were obtained. (III) On the basis of performance assessment and parametric analysis, the multi-objective optimization of the system is carried out considering the game between efficiency and cost to achieve the high-efficiency and low-cost CCHP poly-generation hybrid system.

2. System description and working principle

As shown in Fig 1, the novel combined cooling, heating and power supply system proposed in this work is mainly composed of biomass gasification unit, SOFC unit, HCCI engine unit and absorption refrigeration cycle unit. The working principle of the whole system can be described as follows. The biomass (Stream 1) can be converted into syngas (Stream 4) with the help of the gasifying through the gasification process occurred in the gasifier. The syngas (Stream 4) is separated into impurities, hydrogen (Stream 5) and other mixed gases (Stream 6) by the separator. The mixed gas is fed into reformer to produce more hydrogen by reforming and water gas shift reactions. Then, all the hydrogen fuel and preheated air are fed into SOFC to generate electricity through electrochemical reaction. The SOFC off-gas (Stream 10) is used as the inlet fuel of the engine for additional power generation through the Otto cycle. It should be noted that because SOFC off gas is generally a kind of thin fuel that is somewhat difficult for conventional engines to utilize. HCCI is a new combustion mode based on the gasoline engine, which can make full use of thin fuel for combustion [22]. Herein, the HCCI engine is adopted as the downstream power generation device. The heat of exhaust gas (Stream 11) from the engine is recycled to preheat the air and water. Afterwards the heat of stream 18 is further recycled by the absorption refrigeration (AR) cycle and waste heat collector (WHC) for heating and cooling energy supply.

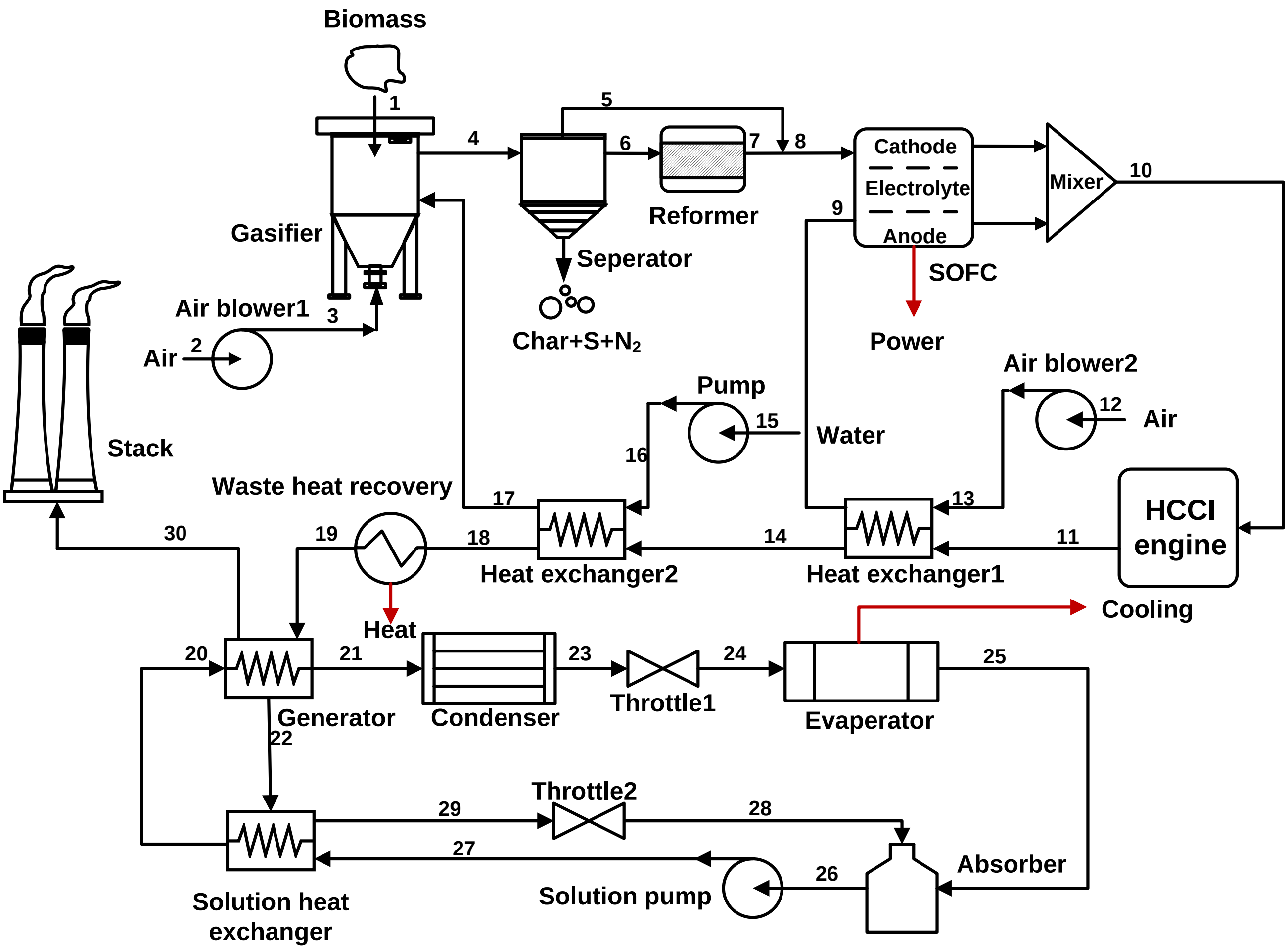

Fig.1 Schematic diagram of CCHP system based on SOFC-Engine and absorption chiller

3. System modeling

3.1. Model assumptions

- The fluid is in a stable flow state and the chemical reaction is in thermodynamic equilibrium state.
- The molar composition of air is presumed of 71% N_2 and 29% O_2 [13,23].
- The system components have good adiabatic performance and the heat loss from the system to the environment can be ignored [23].
- The change in kinetic energy and potential energy can be neglected [13].
- The thermodynamic model is used to model the system components and the thermodynamic parameters are uniformly distributed [24] .

3.2 Thermodynamic model

The chemical process simulation software Aspen Plus is used to model the CCHP system based on biomass fueled SOFC-Engine system. Before setting up the flowsheet of the system, Peng-Robinson equation is selected as the state equation of the fluids. The simulation process of the whole system can be completed after selecting appropriate blocks to model the corresponding components and inputting the composition and flux of the streams. It should be noted that for complex and non-standard database components such as biomass gasifier and SOFC, FORTRAN language needs to be embedded in the appropriate blocks for the components modeling. Finally, in order to make this study easier to be understood and more readable, the process of system modeling and analysis can be described in Fig. 2.

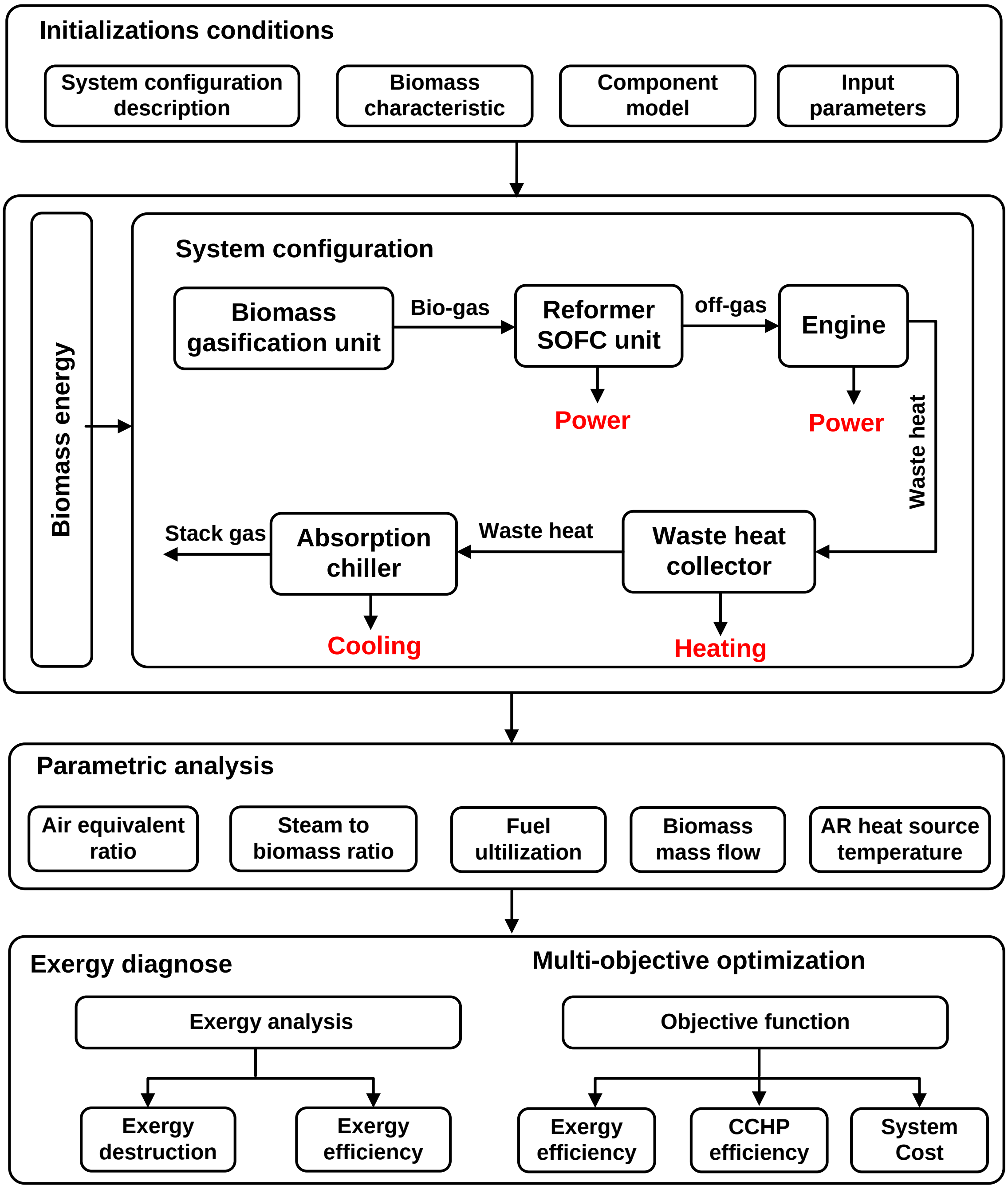

Fig.2 Analysis procedure of the proposed system

3.2.1 Modeling of biomass gasification process

Rice straw from Jiangsu province was adopted as the research case of biomass, and the proximate analysis and ultimate analysis results of biomass are shown in Table 1 [25].

Table 1 The proximate analysis and ultimate analysis of the discussed rice straw biomass [25]

Proximate analysis (wt. %)		Ultimate analysis (wt. %)	
Moisture	9.1	C	35.37
Fixed carbon	16.75	H	4.82
Volatile	63.69	O	39.15
Ash	10.46	N	0.96
Low heating value (MJ/kg)	14.4	S	0.14

The biomass gasification is a relative complex chemical reaction process, which is simulated in two steps. First, the stoichiometric reactor converts all elements of biomass except ash into the elementary substance. The specific process can be described by Eq. (1). Secondly, these basic elementary substances are fed into the Gibbs reactor. The composition of gasification gas at the equilibrium state can be obtained when the reactor reaches the minimum Gibbs free energy.

$$CH_xO_yN_zS_w \rightarrow C + \frac{x}{2}H_2 + \frac{y}{2}O_2 + \frac{z}{2}N_2 + wS \tag{1}$$

where $CH_xO_yN_zS_w$ is the molecular formula of the biomass calculated according to the data in Table 1.

Since the steam and air are adopted as gasification agents, the air equivalent ratio (*ER*) and steam biomass ratio (*S/B*) have great impact on gasification performance. The *ER* is defined as the ratio of the actual amount of air supplied in the gasifier (*AR*) to the amount of air needed for the biomass to achieve complete combustion theoretically (*SR*), as expressed in Eq. (2). Herein, *SR* can be calculated by the element composition of biomass, as shown in Eq. (3). In addition, the steam to biomass ratio (S/B) can be defined as Eq. (4).

$$ER = \frac{AR}{SR} \tag{2}$$

$$SR = \frac{1}{0.21}\left(1.866\omega_C + 5.55\omega_H + 0.7\omega_S - 0.7\omega_O\right) \tag{3}$$

$$S/B = \frac{\text{The mass of steam}}{\text{The mass of biomass}} \tag{4}$$

where ω_C, ω_H, ω_O and ω_N are the mass percentage (%) of carbon, hydrogen, oxygen and nitrogen in the material, respectively.

3.2.2 Modeling of reformer and SOFC

The methane steam reforming (MSR) and water gas shift (WGS) reactions occurring in the reformer can be described in Eqs (5) and (6).

$$\text{MSR:}\quad CH_4 + H_2O \rightarrow CO + 3H_2 \quad \Delta H = 206\ \text{kJ/mol} \tag{5}$$

WGS: $CO+H_2O \rightarrow CO_2+H_2 \quad \Delta H$=-41kJ/mol (6)

The heat released during the fuel cell operation can be calculated according to the Gibbs Helmholtz equation as follows.

$$\Delta H = -nFE + nFT\left(\frac{\partial E}{\partial T}\right)_p \tag{7}$$

where ΔH is the enthalpy of electrochemical reaction; n is the number of transferred electrons; E is electrochemical reaction electromotive force; F is Faraday constant; T is the fuel cell temperature.

The relationship between the actual output voltage V of SOFC and the polarization voltage can be described in Eq. (8). V_{re} is ideal reversible voltage as calculated by Nernst equation [26].

$$V = V_{re} - V_{act} - V_{conc} - V_{ohm} \tag{8}$$

$$V_{re} = E_r^0 - \frac{RT}{4F}\ln\frac{p_{H_2O}^2 p_0}{p_{H_2}^2 p_{O_2}} \tag{9}$$

where V_{act}, V_{conc} and V_{ohm} are activation, concentration and ohm overvoltage, E_r^0 is standard voltage of SOFC, R is ideal gas constant, p is partial pressure of gas, p_0 is standard atmospheric pressure. The calculation of three kinds of overvoltage can be refer to our previous work [14].

The current density of SOFC is written in Eq. (10).

$$J = \frac{I}{NA_c} = \frac{2 \cdot \mu \cdot F \cdot \phi_{H_2}}{NA_c} \tag{10}$$

where μ is fuel utilization factor, φ_{H2} is molar flow of hydrogen fed into SOFC, N is the number of single cell, A_c is the area of single cell.

The output power of SOFC can be calculated in Eq. (11).

$$\dot{W}_{SOFC} = \eta_I \cdot I \cdot V = 2\eta \cdot \mu \cdot F \cdot \phi_{H_2} \cdot V \tag{11}$$

where η_I is efficiency of DC/AC inverter.

3.2.3 Modeling of Engine

The thermodynamic process of the classical Otto cycle is used to approximately model the HCCI engine, which can be generally simplified into sequential working strokes including polytropic compression, constant volume combustion, polytropic expansion, and constant volume exhaust. The exhaust temperature T_{out} and power consumption $\dot{W}_C$ of polytropic compression process can be calculated by Eqs. (12) and (13).

$$T_{\text{out}} = T_{\text{in}} + T_{\text{in}}\left(\gamma^{\varepsilon} - 1\right) \cdot \frac{1}{\eta_{\text{POC}}\eta_{\text{MEC}}} \tag{12}$$

$$\dot{W}_{\text{C}} = \phi \tilde{C}_p T_{\text{in}}\left(\gamma^{\varepsilon} - 1\right) \cdot \frac{1}{\eta_{\text{POC}}\eta_{\text{MEC}}} \tag{13}$$

Correspondingly, the exhaust temperature T_{out} and power generation $\dot{W}_{\text{T}}$ of polytropic expansion process can be calculated by Eqs. (14) and (15).

$$T_{\text{out}} = T_{\text{in}} - T_{\text{in}}\left(1 - \lambda^{\varepsilon}\right) \cdot \eta_{\text{POE}}\eta_{\text{ME}} \tag{14}$$

$$\dot{W}_{\text{E}} = \phi \tilde{C}_p T_{\text{in}}\left(1 - \lambda^{\varepsilon}\right) \cdot \eta_{\text{POE}}\eta_{\text{ME}} \tag{15}$$

where T_{in} is inlet temperature; ϕ is inlet molar flux; γ and λ are compression ratio and expansion; α is polytropic index; η_{POC} and η_{MEC} are polytropic efficiency and mechanical efficiency for compression process; η_{POE} and η_{ME} are polytropic efficiency and mechanical efficiency for expansion process.

3.2.4 Modeling of absorption refrigeration cycle

In the AR cycle, NH_3-H_2O is selected as the working medium because of low price, easy availability, and wide practical scenarios. The AR cycle mainly consists of generator, condenser, evaporator, absorber and solution heat exchanger. Each component should meet the mass balance equation, as shown in Eq. (16) [27].

$$\sum \dot{m}_{\text{in}} x_{\text{in}} = \sum \dot{m}_{\text{out}} x_{\text{out}} \tag{16}$$

where $\dot{m}_{\text{in}}$ and $\dot{m}_{\text{out}}$ are respectively the mass flow of ammonia solution at the inlet and outlet of the component; x_{in} and x_{out} are respectively the concentration of ammonia solution at the inlet and outlet of the component.

The energy conservation equation of each component in the NH_3-H_2O refrigeration cycle is written in Eq. (17) [27].

$$Q_k + \sum \dot{m}_{j,\text{in}} h_{j,\text{in}} = \sum \dot{m}_{k,\text{out}} h_{k,\text{out}} \tag{17}$$

where Q_k is the heat absorbed or released by the ammonia solution; h_{in} and h_{out} are specific enthalpy of ammonia solution at the inlet and outlet of the component, respectively.

Table 2 presents the selection and description of unit operation blocks illustrated in Fig. 1, and these blocks are connected by material, heat or power streams in the simulator.

Table 2 Descriptions of Aspen Plus unit operation models

Component	Aspen Plus block	Description
Gasifier	RSTOIC	Convert the non-conventional stream biomass into conventional components with Fortran language embedded
	RGIBSS	Obtain the gasification gas composition by Gibbs free energy minimum principle
Separator	SSPLIT	Separate the gas from the impurities
Reformer	REQUIL	Simulate the reforming and shift equilibrium reactions
SOFC	RSTOIC	Simulate SOFC working process with Fortran language embedded
Engine	COMPR	Simulate the compression process of engine
	RSTOIC	Simulate the combustion process of engine
	COMPR	Simulate the expansion process of engine
HEX1	HEATX	Heat the SOFC anode inlet air to 800 ^{o}C
HEX2	HEATX	Heat the fresh water to steam required for gasification
WHC	HEATER	Provide the heat power required by the user
Air blower	COMPR	Pressurize the air to provide oxidant to the gasifier and SOFC
Generate	RADFRAC	Desorb ammonia solution to a strong solution and a weak solution
Condenser	HEATER	Condense the strong ammonia solution
Absorb	HEATER	Absorb both strong and weak solutions
Evaporator	HEATER	Evaporate the strong ammonia solution to harvest cooling energy
SHEX	HEATX	Exchange heat between strong solution and a weak solution
Throttle	VALVE	Decompression to obtain low pressure ammonia steam

3.3 Exergy model

The exergy of mixture can be divided into physical exergy and chemical exergy in case of neglecting the macroscopic kinetic energy and potential energy. The physical and chemical exergy can be calculated in Eqs. (18) and (19), respectively.

$$\dot{E}x^{\text{ph}} = \sum_{i=1}^{k}\left[\phi_i\left(h_i - h_0\right) - \phi_i T_0\left(s_i - s_0\right)\right] \tag{18}$$

$$\dot{E}x^{\text{ch}} = \sum_{i=1}^{k}\phi_i x_i ex_i^{\text{ch}} + RT_0\sum_{i=1}^{k}\phi_i x_i \ln x_i \tag{19}$$

where ex_i^{ch} is the specific chemical exergy of composition i, h_i is specific enthalpy of composition i, s_i is the specific entropy of composition i, h_0 and s_0 are the specific enthalpy and entropy of composition i in the environmental state, respectively. The specific chemical exergy of gas can be found in Ref. [28].

For the biomass, the physical exergy is usually neglected and the chemical exergy of biomass can be defined as Eq. (20).

$$\dot{E}x_{\mathrm{bio}} = \beta \dot{m}_{\mathrm{bio}} LHV_{\mathrm{bio}} \tag{20}$$

where $\dot{m}_{\mathrm{bio}}$ is the mass flow rate of biomass; LHV_{bio} is the lower heating value of biomass; β is the multiplication factor, which can be calculated by Eq. (21) [29].

$$\beta = \frac{1.044+0.0160(\omega_{\mathrm{H}}/\omega_{\mathrm{C}})\text{-}0.3493(\omega_{\mathrm{O}}/\omega_{\mathrm{C}})(1+0.0531(\omega_{\mathrm{H}}/\omega_{\mathrm{C}}))+0.0493(\omega_{\mathrm{N}}/\omega_{\mathrm{C}})}{1-0.4124(\omega_{\mathrm{O}}/\omega_{\mathrm{C}})} \tag{21}$$

The thermal exergy resulted from a heat transfer can be written as Eq. (22), according to Carnot's theorem.

$$\dot{E}x_{\dot{Q}} = \dot{Q}\cdot\left(1-T_0/T\right) \tag{22}$$

The definition of exergy destruction $\dot{E}x_{D,k}$, exergy efficiency $\eta_{ex,k}$, exergy destruction ratio y_k and relative exergy destruction ratio y_k^* of each component can be referred to our previous work [14].

3.4 System performance evaluation criteria

The net and gross electrical efficiency of the integrated system can be calculated by Eqs. (23) and (24).

$$\eta_N = \frac{\dot{W}_{\mathrm{SOFC}} + \dot{W}_{\mathrm{Engine}}}{\dot{m}_{bio} LHV_{bio}} \tag{23}$$

$$\eta_G = \frac{\dot{W}_{\mathrm{SOFC}} + \dot{W}_{\mathrm{Engine}} - \dot{W}_{\mathrm{AB}} - \dot{W}_{\mathrm{P}}}{\dot{m}_{\mathrm{bio}} LHV_{\mathrm{bio}}} \tag{24}$$

where $\dot{W}_{\mathrm{AB}}$ and $\dot{W}_{\mathrm{P}}$ are power consumption of air blower and pump, respectively.

The overall energy conversion efficiency (CCHP efficiency) can be written as Eq. (25).

$$\eta = \frac{\dot{W}_{\mathrm{SOFC}} + \dot{W}_{\mathrm{Engine}} + \dot{W}_{\mathrm{Q}} + \dot{W}_{\mathrm{C}} - \dot{W}_{\mathrm{AB}} - \dot{W}_{\mathrm{P}}}{\dot{m}_{\mathrm{bio}} LHV_{\mathrm{bio}}} \tag{25}$$

where $\dot{W}_{\mathrm{Q}}$ and $\dot{W}_{\mathrm{C}}$ are heating power from waste heat collector and cooling power produced by AR cycle.

The exergy efficiency of this hybrid system of the proposed model is defined as Eq. (26).

$$\eta_{ex} = \frac{\dot{W}_{\mathrm{SOFC}} + \dot{W}_{\mathrm{Engine}} + \dot{E}x_{\mathrm{Q}} + \dot{E}x_{\mathrm{C}} - \dot{W}_{\mathrm{AB}} - \dot{W}_{\mathrm{P}}}{\dot{E}x_{\mathrm{bio}}} \tag{26}$$

where $\dot{E}x_{\mathrm{Q}}$ and $\dot{E}x_{\mathrm{C}}$ are heating and cooling exergy.

Primary energy rate (PER) refers to the ratio of primary energy consumption to output energy. This parameter indicates that the amount of primary energy consumed by the system when the energy output demand is specified. The PER of the CCHP system can be calculated as Eq. (27). The PER of the independent production system can be calculated by Eq. (28).

$$PER_{\mathrm{C}} = \frac{Q_{\mathrm{P}}}{\sum Q_{\mathrm{C}} + \sum Q_{\mathrm{H}} + \sum P_{\mathrm{E}}} \tag{27}$$

$$PER_{\mathrm{I}} = \frac{\sum Q_{\mathrm{C}} / \eta_{\mathrm{c}} + \sum Q_{\mathrm{H}} / \eta_{\mathrm{h}} + \sum P_{\mathrm{E}} / \eta_{\mathrm{e}}}{\sum Q_{\mathrm{C}} + \sum Q_{\mathrm{H}} + \sum P_{\mathrm{E}}} \tag{28}$$

where $\sum Q_{\mathrm{H}}$, $\sum Q_{\mathrm{C}}$ and $\sum P_{\mathrm{E}}$ are the total heating, cooling and power output of the system, respectively; Q_{P} is primary energy consumption of CCHP system; η_{e}, η_{h} and η_{c} are efficiency of electrical grid, boiler efficiency of district heating and refrigeration efficiency, respectively. The efficiency of electrical grid and boiler is set as 0.33 and 0.85, while the COP of electric compression refrigerator is set as 4.5 [30].

The primary energy saving ratio (PESR) of the CCHP system compared with the independent production system is defined as:

$$PESR = 1 - \frac{PER_{\mathrm{C}}}{PER_{\mathrm{I}}} \tag{29}$$

4 Methods of optimization and decision-making

Considering the game between cost and efficiency, the system is optimized with the minimum cost and the maximum efficiency. Through the multi-objective optimization, it is expected to provide a reference value for the optimal operating point to achieve high efficiency and low cost in the meanwhile.

4.1 Objective function

The first objective function is to maximize the exergy efficiency of the system, and the specific expression is consistent with Eq. (30).

$$Obj.Func.I = \eta_{ex} \tag{30}$$

The second objective function is to maximize the overall energy conversion efficiency (CCHP efficiency) of the system. The specific expression is consistent with Eq. (31).

$$Obj.Func.II = \eta \tag{31}$$

The last objective function is to minimize the total annual cost (*TAC*), as expressed in Eq. (32). The TAC includes the annual operation cost, the annual maintenance cost, the annual investment interest, the annual insurance, and the tax per annum, as shown in Eq. (33). The capital cost of all components, whose model can refer to Appendix A, is allocated to the annual depreciation cost based on the operating life of the system. The cost models of the six different parts are summarized in Table 3.

$$Obj.Func.III = TAC \tag{32}$$

$$TAC = C_{\mathrm{Dep}} + C_{\mathrm{Ope}} + C_{\mathrm{Mai}} + C_{\mathrm{Int}} + C_{\mathrm{Ins}} + C_{\mathrm{Tax}} \tag{33}$$

Table 3 The annual cost models involved in the CCHP system [31,32]

Annual cost composition	Model equation	Parameter
Depreciation cost C_{Dep} (\$/year)	$C_{\mathrm{Dep}} = \frac{C_{\mathrm{Cap}}}{\lambda}$	λ: cycle life, 10 years
Operation cost C_{Ope} (\$/year)	$C_{Ope} = \dot{m}_{\mathrm{bio}} \cdot \pi_{\mathrm{bio}} \cdot \frac{t_{Ope}}{\lambda}$	$\dot{m}_{\mathrm{bio}}$: Biomass flux, kg/h π_{bio}: Biomass price, 0.124 \$/Nm^3 t_{ope}: Total operating time, 8000 h
Maintenance cost C_{Mai} (\$/year)	$C_{\mathrm{Mai}} = \frac{C_{\mathrm{Cap}}}{\lambda} \cdot f_{\mathrm{Mai}}$	f_{Mai}: Maintenance factor, 0.06
Investment interest cost C_{Int} (\$/year)	$C_{\mathrm{Int}} = \frac{C_{\mathrm{Cap}}}{\lambda} \cdot f_{\mathrm{Int}}$	f_{Int}: Interest factor, 0.0926
Insurance cost C_{Ins} (\$/year)	$C_{\mathrm{Ins}} = \frac{C_{\mathrm{Cap}}}{\lambda} \cdot f_{\mathrm{Ins}}$	f_{Ins}: Insurance factor, 0.20
Tax cost C_{Tax} (\$/year)	$C_{\mathrm{Tax}} = \frac{C_{\mathrm{Cap}}}{\lambda} \cdot f_{\mathrm{Tax}}$	f_{Tax}: Tax factor, 0.054

4.2 Decision variables

To optimize the integrated system, the relevant decision variables should be selected and specified. According to the system configuration and parametric analysis, biomass mass flux $\dot{m}_{bio}$, biomass conversion ratio α, SOFC fuel utilization ratio μ, air equivalent ratio *ER*, steam biomass ratio *S/B* and outlet temperature of WHC T_{W} are selected as the decision variables. The value range of specific operation variables is shown in Table 4.

Table 4 Optimization ranges of the selected decision variables

Decision variable	Unit	Description	Range of design variable	
			Upper limit	Lower limit
$\dot{m}_{\text{bio}}$	kg/h	System biomass feed mass flow rate	400	600
α	/	Biomass conversion ratio in gasification process	0.9	1.0
μ	/	The utilization factor of SOFC	0.5	0.85
ER	/	Air equivalent ratio	0.05	0.20
S/B	/	Steam to biomass ratio	0.6	1.0
*T*w	°C	Waste heat collector outlet temperature	200	300

4.3 Decision making

How to select the optimum point in Pareto frontier is an important problem in the multi-objective optimization method. In this study, the well-known LINMAP (Linear Programming Technique for Multidimensional Analysis of Preference) method was applied to make the decision and select the optimum solution. First, the solutions on the Pareto frontier should be normalized by Eq. (34). Then the Euclidian distance (ED_{i+}) between each point on Pareto frontier and ideal point is defined in Eq. (35), thus the point on Pareto frontier with the shortest distance is considered as the prior optimal point [33].

$$f_{ij}^{\text{norm}} = \frac{f_{ij} - \min(f_{ij})}{\max(f_{ij}) - \max(f_{ij})} \tag{34}$$

$$ED_{i+} = \sqrt{\sum_{j=1}^{n} \left(f_{ij}^{\text{norm}} - f_{j}^{\text{ideal}} \right)^2} \tag{35}$$

where *j* is the number of optimize objectives and *i* is the number of points on the Pareto frontier.

Multi-objective optimization is achieved by writing the NSGA-II algorithm program in MALAB© 2014a environment to call Aspen Plus. The main parameters involved in the process of thermodynamic modeling and multi-objective optimization are summarized in Table 5. In addition, the thermodynamic state of each stream of the system can be found in Appendix B.

Table 5 The main parameters involved in the simulated and optimized process

Parameter	value
Gasification unit	

Operation pressure of gasifier p_b	5 bar
Temperature of inlet stream of gasifier T_s	300 °C
Biomass conversion ratio α_B	0.95
Polytrophic efficiency of air blower η_p	0.9
Mechanic efficiency of air blower η_M	0.95
Efficiency of water pump η_W	0.9
Efficiency of pump driver η_D	0.95
Reformer SOFC unit	
Operation pressure of reformer	5 bar
Operation pressure of SOFC	5 bar
Cell numbers	40000
Single cell area A_a	0.01 m^2
DC/AC invert efficiency η_I	0.95
Engine unit	
Polytropic efficiency of the compression process η_{POC}	0.9
Mechanical efficiency of the compression process η_{MEC}	0.95
Compression ratio	4.4
Polytropic efficiency of the expansion process η_{POE}	0.9
Mechanical efficiency of the expansion process η_{ME}	0.95
Combustion conversion rate α_C	1.0
Absorption refrigeration cycle	
Number of generator stages N_G	8
High pressure p_h	15.56 bar
Low pressure p_l	2.5 bar
Concentration of strong solution C_s	96.1%
Concentration of weak solution C_w	33.6%
Exergy analysis	
WHC efficiency	0.75
AR temperature	10 °C

AR ambient temperature	50 °C
Ambient temperature T_0	20 °C
Ambient pressure p_0	1 bar
Multi-optimization analysis	
Population size	60
Number of genetic generation	30

5 Results and discussion

5.1 Model Validation

The developed model of the hybrid system is verified by comparing the three different unit model results with the experiment or reported data. First, the simulation results of biomass gasification in this work were compared with the experimental results of Fremaux et al. [34], as shown in Fig 3. To make the comparison, the input parameters of the model have been set consistent with the experimental conditions. The experimental and simulated results of hydrogen yield are in good agreement under the reaction temperature of 900 °C. However, when the reaction temperature is 700 °C, the simulated hydrogen concentrations is somewhat higher than experiment, especially at low S/B. This is mainly because the production of tar and high-carbon hydrocarbons is not taken into account in the model, which is also discussed in our previous work and other relative reports [14,35]. In general, the model is reliable enough to predict the biomass gasification process.

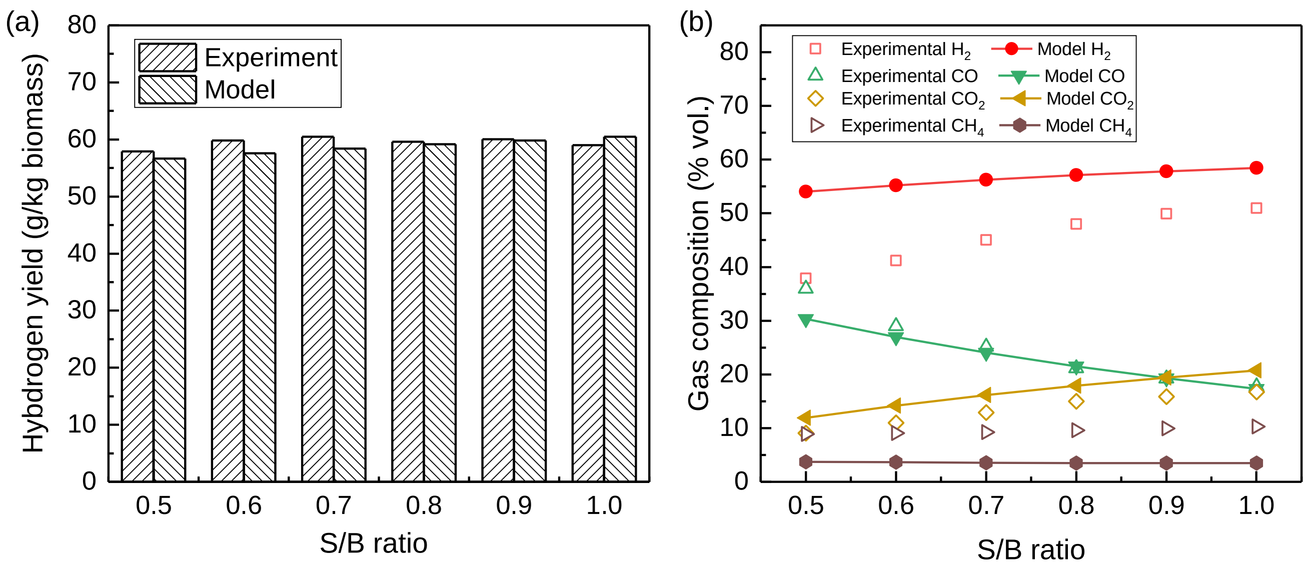

Fig. 3 (a) Hydrogen yield comparison of experiment and simulation result at 900 °C; (b) Gas composition comparison of experiment and simulation result at 700 °C

The SOFC model is also validated by comparing the simulation and experiment results, as shown in Fig 4. The experiment [36] and simulation results of SOFC agree well, indicating that the model is reliable enough to predict the SOFC performance. The absorption refrigeration cycle model refers to the book of “Absorption chillers and heat pumps” [37] and the stream thermodynamic data was adjusted to improve the COP.

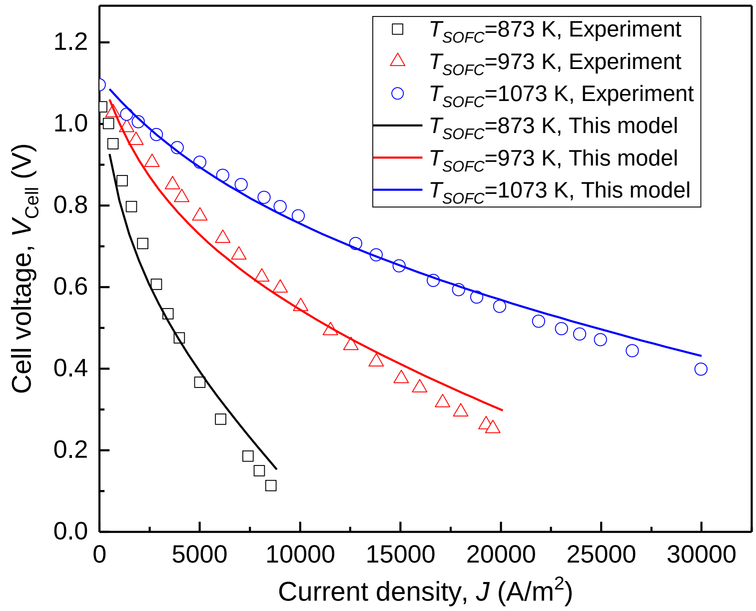

Fig.4 The verification of SOFC model [36]

5.2 Energy performance

As listed in Table 6, the polygeneration system can generate electric power of 1085 kW, heating power of 250 kW, and cooling power of 99 kW under the initially given operating conditions with the biomass feed of 500 kg·h^{-1}. The output power of SOFC and engine is 721 kW and 364 kW, respectively. The auxiliary power required by the blowers and pumps is 85 kW. Accordingly, the gross electrical efficiency and net electrical efficiency of the system are calculated to be 54.3% and 50.0%, respectively. The CCHP efficiency is 67.5% in total. It is worth noting that the PESR of the CCHP system is 41%, which means that the PER of the poly-generation system is significantly lower than that of the independent system. For example, the boiler, electric compression refrigerator and centralized electrical grid are adopted for separate energy supply. Although the poly-generation system uses a single-effect ammonia absorption chiller with a performance coefficient of only 0.52, the entire system still has a low primary energy consumption rate, because the heat required by the refrigeration cycle comes from the exhaust heat. In general, the CCHP system exhibits relatively great energy saving potential.

Table 6 The energy performance of the CCHP system with the biomass feed of 500 kg/h at the typical operation conditions

Item	Input power	Electrical power		Heating power	Cooling power	Auxiliary power	Efficiency			PESR
		SOFC	Engine				η_N	η_G	η	
Value	2000 kW	721 kW	364 kW	250 kW	99 kW	85 kW	50.0 %	54.3%	67.5%	41%

5.3 Parametric analysis

In order to optimize the performance of the design system, this section discusses the influence of the main parameters like *ER*, *S*/*B*, fuel utilization of the SOFC, etc., on the performance of the system. Fig. 5 displays the variation trend of the system output power and efficiency with the increase of biomass flux. When the biomass feedstock increases from 400 to 600 kg/h, the output electric power increases from 795.6 to 1193 kW, and the thermal power increases from 84.6 to 428 kW. The cooling power remains essentially unchanged due to the hot source stream temperature T_{19} of the AR subsystem is specified. Since the biomass feedstock flow has little impact on the performance of power generation equipment, the power generation efficiency of the system basically remains unchanged. However, the CCHP efficiency of the system has a significant improvement due to the large increase in the thermal output power. Accordingly, the system exergy efficiency also gradually increases. This means that the large-scale system helps to reduce exergy loss and improve overall energy utilization efficiency.

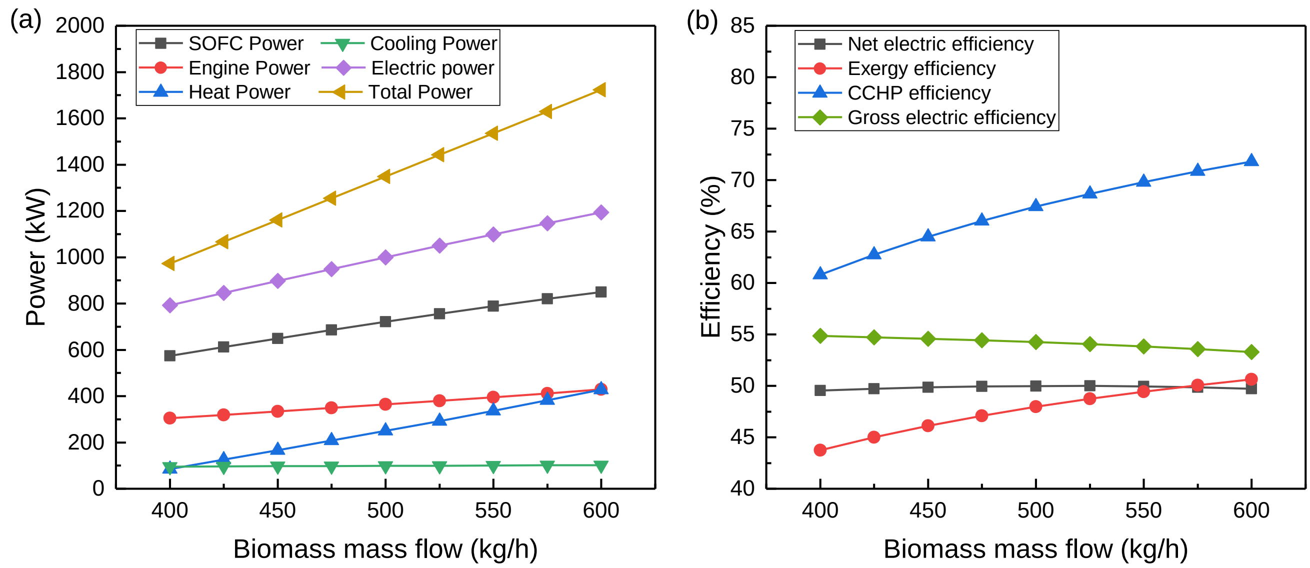

Fig .5 Effects of biomass mass flow on system performance

Fig. 6 describes the effect of *S*/*B* on the electrical power, heating power, cooling power and various efficiencies of the system. As is depicted in Fig. 6a, with the increase of *S*/*B* ratio from 0.5 to 1.0, the electrical power output of the system gradually increases from 1074.9 to 1112.1 kW. Accordingly, the gross electrical efficiency increases from 53.7% to 55.6%. The upward trend of the output electrical power can be explained as follows. The increase of steam flow is conducive to the forward movement of water gas shift reaction of carbon monoxide converting into hydrogen, so that the contents of hydrogen and carbon dioxide increase, while the content of carbon monoxide decreases. The increase in hydrogen fuel leads to an increase in the electrical power generated by SOFC. The SOFC is the main power generation device, so the electrical power and efficiency of the system increase gradually. Meanwhile, the output heating power decreases continuously to a large extent from 301.9 to 55.0 kW. As a result, the total output power and the CCHP efficiency also decrease gradually. The increase of *S*/*B* means that the exhaust gas flow providing the heat to the absorption chiller increases. However, due to the determination of the heat source temperature for the absorption chiller, the output cooling power increases slightly from 96.5 to 107.4 kW.

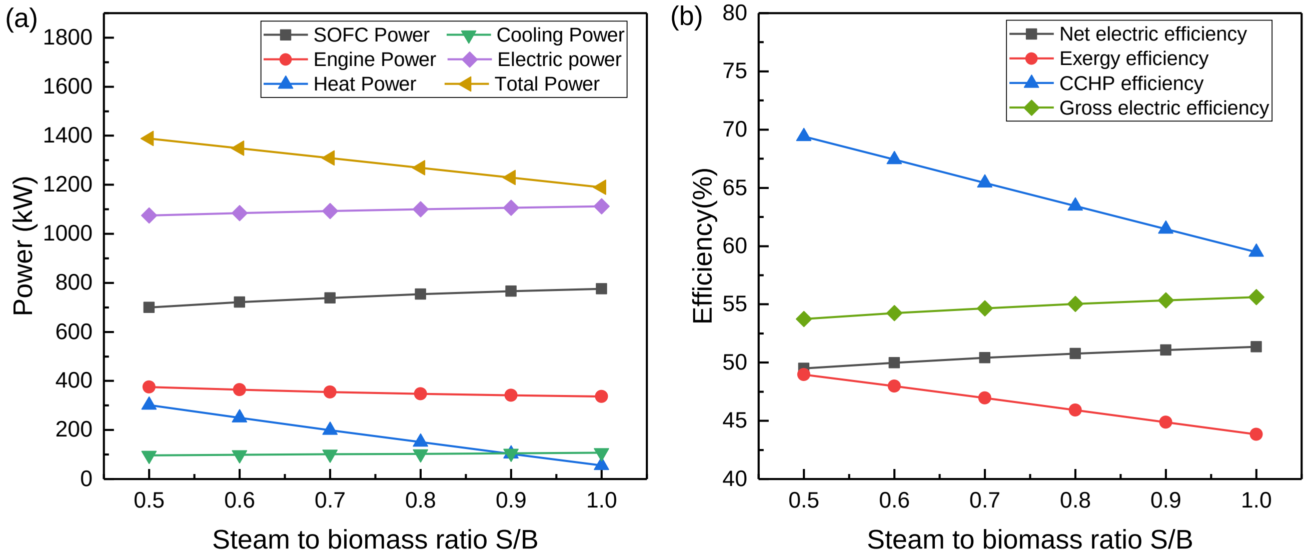

Fig. 6 Effects of steam to biomass ratio *S*/*B* on system performance

Air equivalent ratio *ER* is another important parameter affecting the biomass gasification process. Fig. 7 depicts the effects of *ER* on the output power and efficiency of the system. With the increase of *ER* from 0.05 to 0.20, the total output power of the system decreases from 1379.2 to 1308.2 kW, and the net electrical power decreases from 1033.4 to 899.2 kW. The heating power slightly decreases first and then increases, while the cooling power remains basically unchanged at about 98 kW. When *ER* is less than 0.1, the SOFC output power gradually increases. The output power of engine and heat power decreases. As *ER* increases gradually until over 0.1, SOFC output power shows a downward trend while engine output power and thermal power increase. This phenomenon is mainly due to the increase of *ER*, which leads to the increase of oxygen flow fed into the gasifier. Correspondingly, the temperature of the gasifier increases, and the water gas shift reaction of carbon monoxide and stream moves toward the positive direction, which facilitates to the hydrogen production. Furthermore, the hydrogen-oxygen reaction consumes a certain amount of hydrogen, resulting in a slight decrease in the concentration of hydrogen input to the SOFC. As *ER* continues to increase, the reaction between hydrogen and oxygen will intensify, resulting in a significant drop in hydrogen content. Therefore, the output power of SOFC decreases slowly and then greatly decreases. From the perspective of efficiency, the electrical efficiency and exergy efficiency of the system remain unchanged and then decrease continuously when *ER* is less than 1.0. The CCHP efficiency reduces gradually from 69.0% to 65.4%.

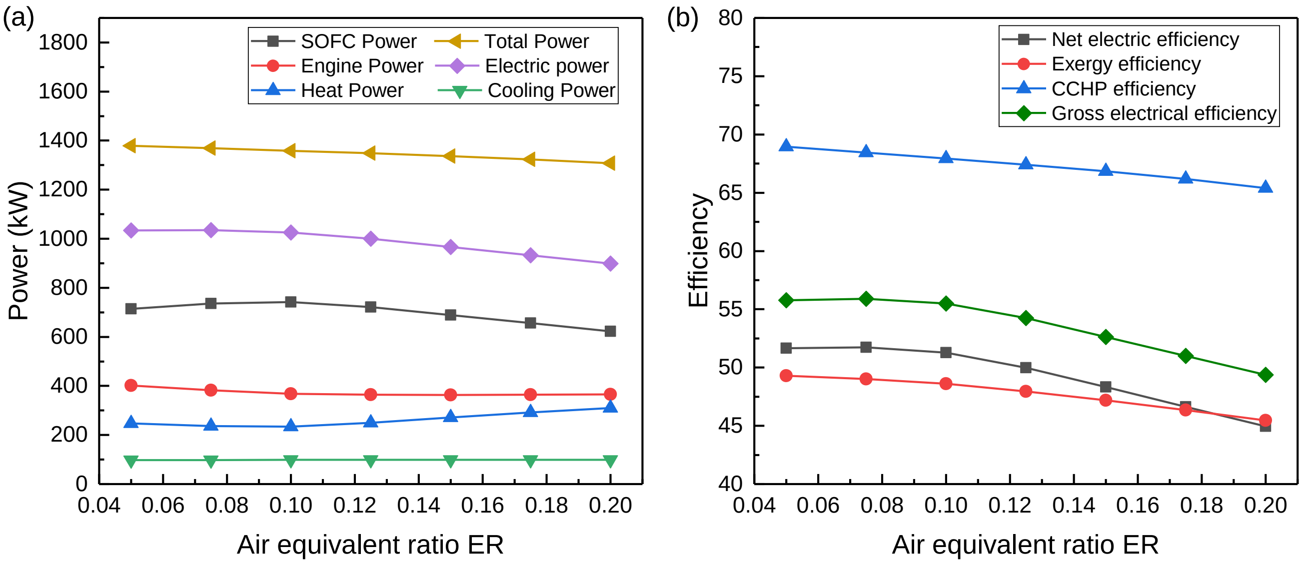

Fig. 7 Effects of air equivalent ratio *ER* on system performance

Fuel utilization factor μ is an important parameter of SOFC. Fig. 8 illustrates the influence of μ on the system-energy conversion performance. As the fuel utilization increases, both the exergy efficiency and generation efficiency of the system gradually increase. When the fuel utilization factor increases from 0.5 to 0.85, the net and gross electrical efficiencies increase from 45.7% to 50.0% and from 50.0% to 53.2%, respectively. The increase in the fuel utilization factor means that more hydrogen participates in the electrochemical reaction, which increases the output power of the SOFC. However, increasing the fuel utilization makes the output power of engine decrease. Since the efficiency of SOFC is generally much higher than that of engines, the increment of SOFC output power is larger than the decrement of engine power. In terms of the whole system, this feature decides the increase of electrical power and electrical efficiency of the proposed hybrid system. The fuel utilization factor μ only changes the fuel flow into the SOFC and the engine, thereby affecting the power ratio of the SOFC to the engine, but has no impact on the biomass gasification process. Therefore, the total energy conversion efficiency of the system remains basically unchanged at around 68%.

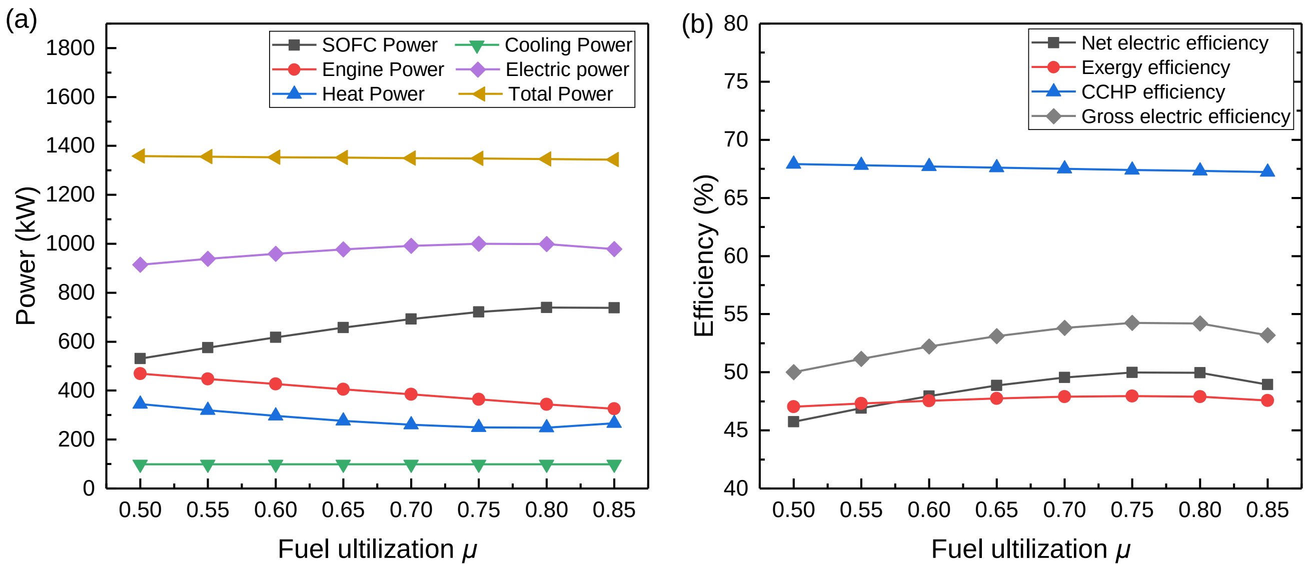

Fig. 8 Effects of fuel utilization factor μ of SOFC on system performance

Fig. 9 discusses the effects of the heat source temperature on the performance of the absorption refrigeration cycle. With the increase of AR heat source temperature T_{19}, the output cooling power from the AR cycle increases from 59.9 to 137.0 kW, while the output heating power decreases from 318 to 180.7 kW. Since the efficiency of the AR cycle is only about 0.5, the CCHP efficiency is reduced from 68.9% to 65.9%, correspondingly. At the same time, the increase of the temperature of No.19 stream makes the heat output from waste heat collector reduce. Although the input heat exergy to AR cycle is increased, the efficient is relatively low. Therefore, the overall exergy efficiency of the system is reduced. Moreover, the distribution of thermal power and cold power of the system can be adjusted by changing the AR cycle heat source temperature, so as to meet the energy demand in different occasions.

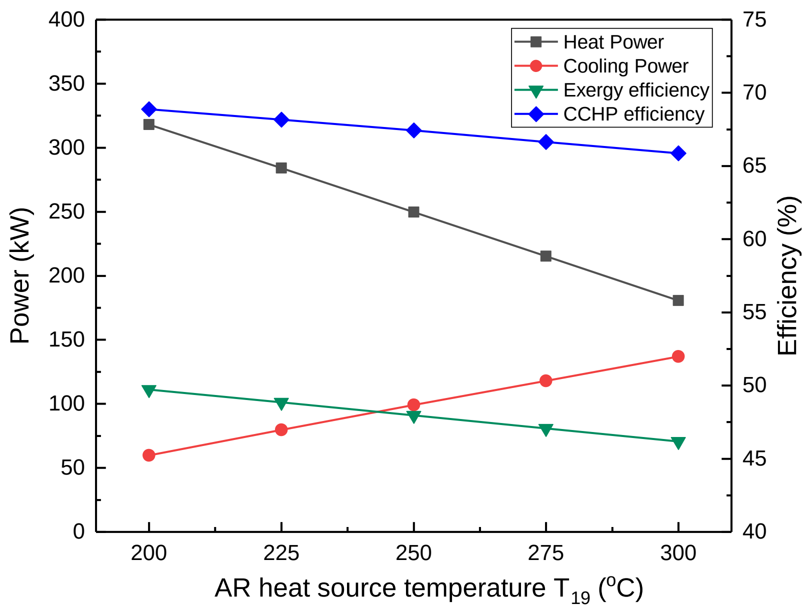

Fig. 9 Effects of AR heat source temperature T_{19} on system performance

5.4 Exergy analysis

The first law of thermodynamics can only give the energy flow of the system, but cannot further give the irreversible loss of the system. The second law of thermodynamics analysis, also namely exergy analysis, can not only give the irreversibility of each component, but also the contribution of the component exergy destruction to the total exergy destruction of the entire system. The exergy performance including exergy destruction $\dot{E}x_{D,k}$, exergy efficiency $\eta_{ex,k}$, and exergy destruction ratio y_k of each component are summarized in Table 7**.** As seen from the table, the overall exergy efficiency of the CCHP system is 45.7%, which is slightly lower than the energy conversion efficiency due to the irreversibility of energy conversion process. Meanwhile, the exergy efficiency and relative exergy destruction of each component involved in the system can be obtained. The detailed exergy information could provide a feasible direction for subsequent optimization of the system: focusing on the components with high relatively exergy destruction ratio and low exergy efficiency. For example, in the system, the exergy efficiency of gasifier, heat exchangers and engine is relatively low. The exergy destruction of gasifier reaches up to 511.66 kW with the exergy efficiency of 79.6%, whose relative destruction ratio is 46.9%. This is mainly because that complex chemical reactions occur in the gasifier, resulting in a large irreversible loss. The exergy destructions of HEX1, HEX2 and WHC are 234.9 kW with the relative exergy destruction ratio of 21.5% in total. The exergy destruction of heat exchange equipment is mainly caused by the large heat transfer temperature difference between the inlet and outlet fluids. The engine is another component with a large exergy loss (182.9 kW) and the exergy efficiency of 66.6%. By comparison, the SOFC has a small exergy destruction (69.92 kW) and high exergy efficiency (91.2%). The comparison results indicate that the SOFC generates electricity with high efficiency in a small exergy destruction, which further reflects the advantages of SOFC as next power generation technology. In the refrigeration cycle, the components with large exergy destruction include evaporate and absorber, whose exergy destruction are 13.6 and 20.3 kW. The evaporator is a component that generates cooling energy, but the grade of the required indoor cooling is low. That's also why the exergy efficiency is low. In addition, the absorber takes the exergy destruction of the mixing process into account.

Table 7 The exergy analysis results of the proposed biomass based SOFC-Engine hybrid CCHP system

Component, k	$\dot{E}x_{F,k}$ (kW)	$\dot{E}x_{P,k}$ (kW)	$\dot{E}x_{D,k}$ (kW)	$\eta_{ex,k}$ (%)	y_k (%)	y_k^* (%)
Gasifier	2505.44	1993.77	511.66	79.58	20.42	46.86
Separator	60.00	57.99	2.01	96.64	3.36	0.18
Air blower1	5.00	4.25	0.75	85.00	15.00	0.07

Reformer	760.90	755.01	5.89	99.23	0.77	0.54
SOFC	790.97	721.05	69.92	91.16	8.84	6.40
Engine	546.94	364.00	182.94	66.55	33.45	16.75
Air blower2	75.00	64.88	10.12	86.51	13.49	0.93
HEX1	537.83	412.89	124.93	76.77	23.23	11.44
Pump	0.04	0.04	0.00	99.81	0.19	0.00
HEX2	160.17	75.78	84.39	47.31	52.69	7.73
WHC	129.42	103.88	25.55	80.26	19.74	2.34
Generate	66.51	54.87	11.64	82.50	17.50	1.07
Condenser	34.65	22.91	11.74	66.11	33.89	1.08
Throttle1	22.91	21.24	1.67	92.70	7.30	0.15
Evaporator	24.74	11.15	13.59	45.05	54.95	1.24
Absorber	25.45	5.16	20.30	20.26	79.74	1.86
Solution Pump	5.00	1.88	3.12	37.63	62.37	0.29
SHEX	51.77	40.76	11.01	78.73	21.27	1.01
Throttle2	5.38	3.91	1.48	72.59	27.41	0.14
Total	-	-	1092.01	-	-	1000
System level	2421.60	1106.93	1314.68	45.71	54.29	-

In order to intuitively understand the exergy flow of each component in the system, the exergy flow diagram (Sankey diagram) is drawn according to the exergy results, as shown in Fig 10. It is particularly noted that since no chemical reaction is involved in the absorption refrigerating cycle, chemical exergy of streams is not considered in the absorption refrigeration cycle in order to simplify the process of exergy analysis. In this Sankey diagram, the black block represents the specific component, and the red arrow represents the exergy flow carried by the stream. The exergy flow of the entire system starts from the inlet biomass exergy. The exergy flow passing through every component will produce the corresponding exergy destruction. That's to say, the value of exergy flow will gradually decrease. The exergy fuel, exergy product and exergy destruction of each component can also be easily and conveniently acquired through this Sankey diagram. For example, for a biomass gasifier, the exergy fuel is the sum of No.1, No.17, and No.3 streams, which is 2505.4 kW. The exergy product is the exergy flow of stream No.4, which is 1975.2 kW. Naturally, the exergy destruction of gasifier (marked as D_Gasifier in Fig 10) is the difference between exergy fuel and exergy product, which is 511.7 kW.

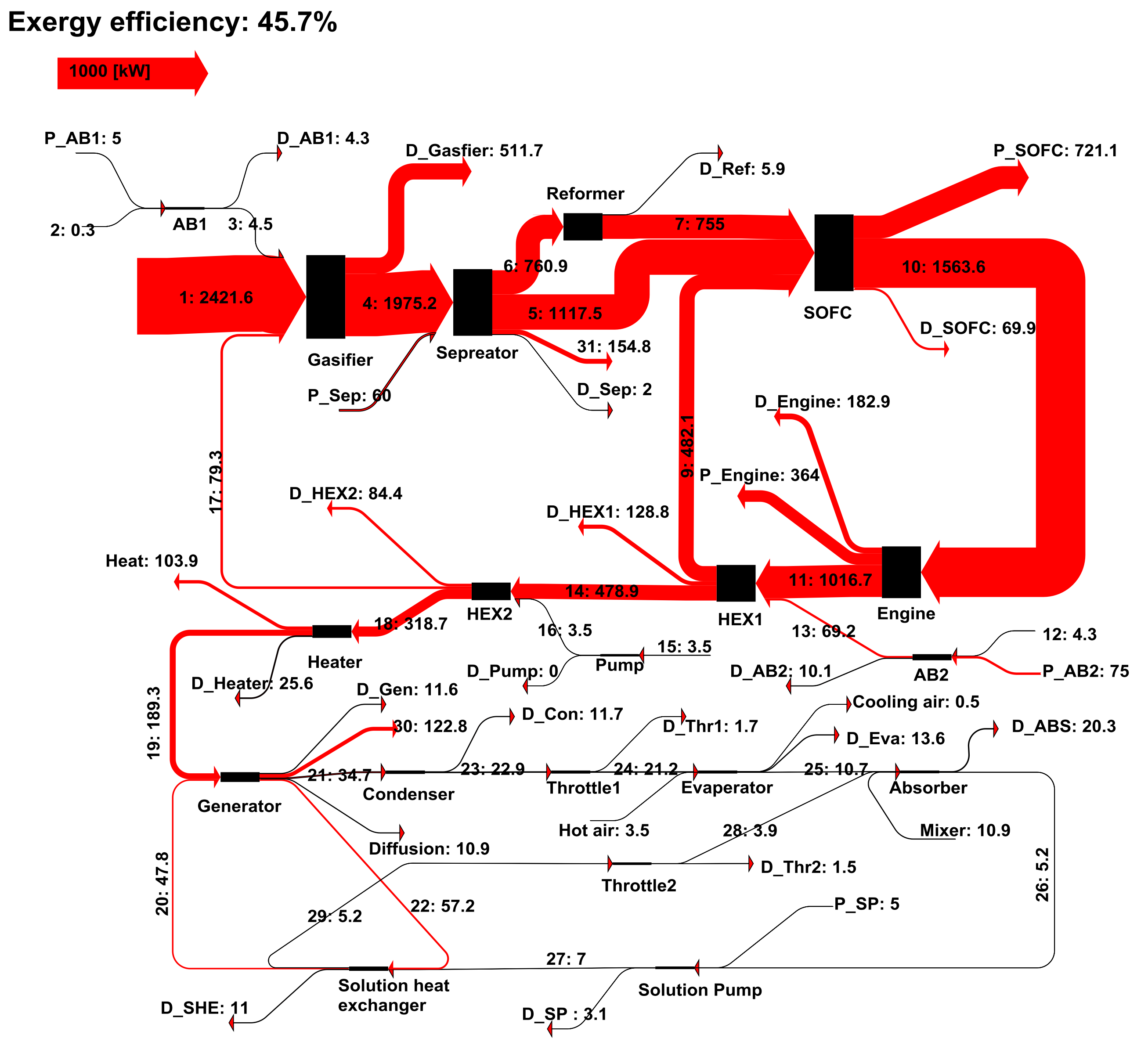

Fig. 10 Sankey diagram to show the exergy flow through the proposed hybrid system

5.5 Pareto frontier and optimum solution

The multi-objective optimization considers the tradeoff between high efficiency and low cost. The Pareto frontier determined by NSGA-II algorithm shows the game between efficiency and cost. Fig. 11 shows the Pareto frontier considering the objective function I (maximum exergy efficiency) and objective function III (TAC). The Pareto frontier considered Function II: maximum CCHP efficiency and Function III: TAC is depicted in Fig 12. On the Pareto front, each point represents a non-dominated solution. In Fig 11, Point B, which has the shortest Euclidean distance from the idea solution, is the optimum solution obtained through multi-objective optimization. In this case, the optimum solution is the exergy efficiency of 50.3% and the TAC of 401 k$. The point A shows the lowest exergy efficiency (43.7%) and also the lowest TAC (389 k$), which effectively realizes the single-objective optimization of objective function III. In the same way. the exergy efficiency of 52.1% is the highest but the economic performance with TAC of 463 k$ is the worst at Point C, which is equivalent to the single-objective optimization of objective function I. Compared with these two feasible solutions considering a single objective function, the exergy efficiency of the optimum solution (Point B) increases by 3.5% and the TAC decreases by 15.9%. The relation between exergy efficiency and TAC is fitted, the fitted curve is expressed as Eq. (36). Similarly, Fig. 12 considers the bio-objective optimization between CCHP efficiency and TAC. The point E is the optimal solution with the CCHP efficiency of 75.0% and TAC of 410 k$. By comparison, the point D is the result of single-objective optimization using TAC as target, where the exergy efficiency is 62.7% and TAC is 385 k$. The point F is the non-dominated solution with the highest CCHP efficiency of 77.2% but with the highest TAC of 572 k$. It is obvious that the increase in efficiency comes at the expense of increasing TAC. The fitting curve expression between CCHP efficiency and TAC is shown in Eq. (37). In summary, the values of design variables and the corresponding performance optimization results for points A-C and D-F are given in detail in Table 8.

$$TAC = 39.3 + 13740 / (1 + 10^{(59-\eta_{ex})\times 0.486}) \tag{36}$$

where $43.7\% \le \eta_{ex} \le 52.1\%$ R^2=0.974

$$TAC = 39.03 + 10^{-43} e^{\eta/0.763} \tag{37}$$

where $62.7\% \le \eta \le 77.2\%$ R^2=0.934

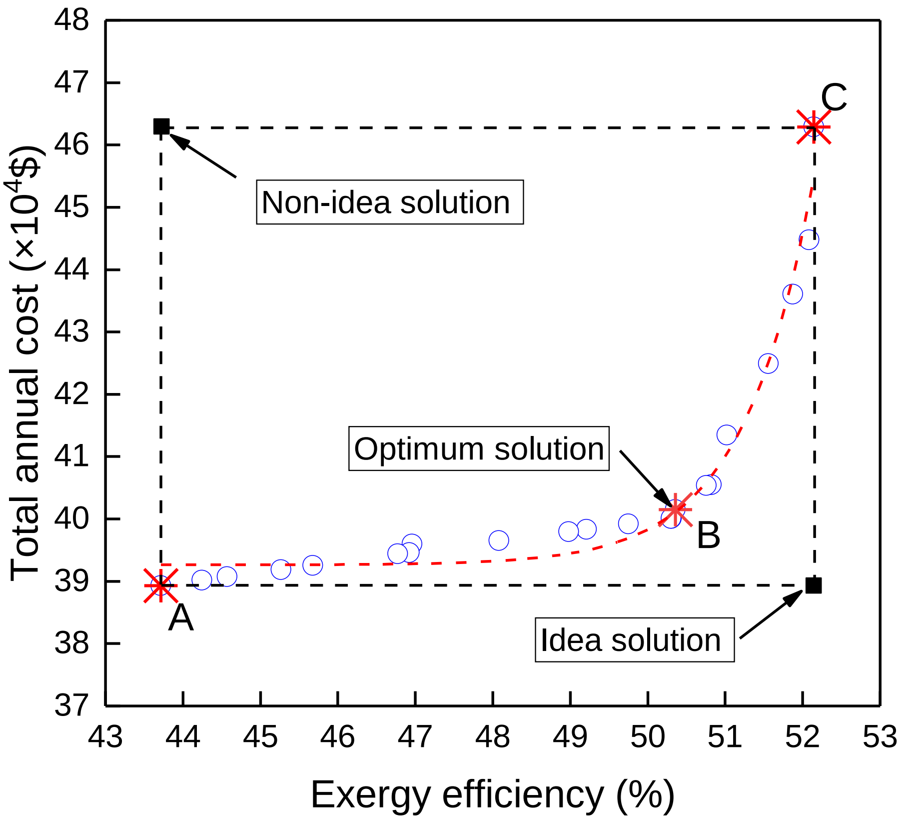

Fig. 11 Pareto frontier of exergy efficiency and TAC

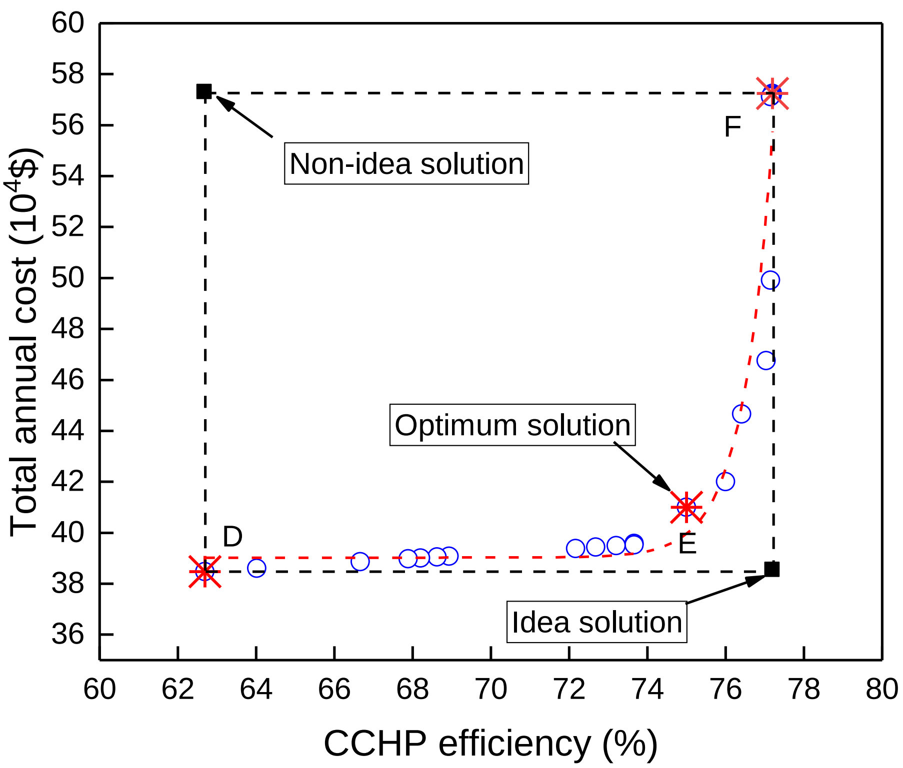

Fig. 12 Pareto frontier of CCHP efficiency and TAC

Table 8 The values of objective functions and operation variables at points A-C and D-E

	Unit	A	B	C	D	E	F
Operation variables							
$\dot{m}_{bio}$	kg/h	515.1	541.1	553.02	455.0	589.1	597
α	/	0.9	0.987	1.0	0.9	0.987	1.0
μ	/	0.5	0.5	0.747	0.5	0.5	0.85
ER	/	0.0852	0.0915	0.0766	0.0745	0.0516	0.05
S/B	/	0.741	0.618	0.798	0.798	0.724	0.664
Tw	°C	201	282	265	292.7	299.4	300
Objective functions							
Exergy efficiency	%	43.7	50.3	52.1	-	-	-
CCHP efficiency	%	-	-	-	62.7	75.0	77.2
TAC	k$	389	401	463	385	410	572

The energy performance of different CCHP systems based on biomass is also compared and shown in Fig. 13. The electrical efficiency (more than 50%) of this system is much higher than other biomass-based ICE, SE and turbine systems and comparable to other SOFC systems, indicating that the integration of biomass and SOFC to form a CCHP system is a relatively efficient energy conversion configuration. This is mainly because SOFC itself has high electrical and thermal efficiency while conventional thermal engines are mostly electrical inefficient, which also highlights the advantages of SOFC as a next-generation power generation device. In addition, it is worth noting that the CCHP efficiency of the proposed system is lower than that of some integrated systems, such as SOFC+ORC+AR. This comparison result is caused by the partly thermal energy of the exhaust gas of the system is recycled to produce the cooling power through the NH_3-H_2O AR cycle. Generally speaking, the efficiency of AR cycle using NH_3-H_2O as working medium is around 0.52 [38], which is lower than that of LiBr-H_2O AR cycle (around 0.7). Meanwhile, the heat source temperature of NH_3-H_2O AR system is higher, so the utilization of low-grade waste heat is not as sufficient as that of LiBr-H_2O AR cycle. Therefore, the CCHP efficiency of this system is lower than that last two integrated energy system using LiBr-H_2O as AR cycle working fluid in Fig. 13. After multi-optimizing the system, the system could reach a relative higher CCHP efficiency of 75% compared with other CCHP systems. On the whole, the CCHP system proposed in this work not only has a higher electrical efficiency but also maintains a better comprehensive energy conversion performance.

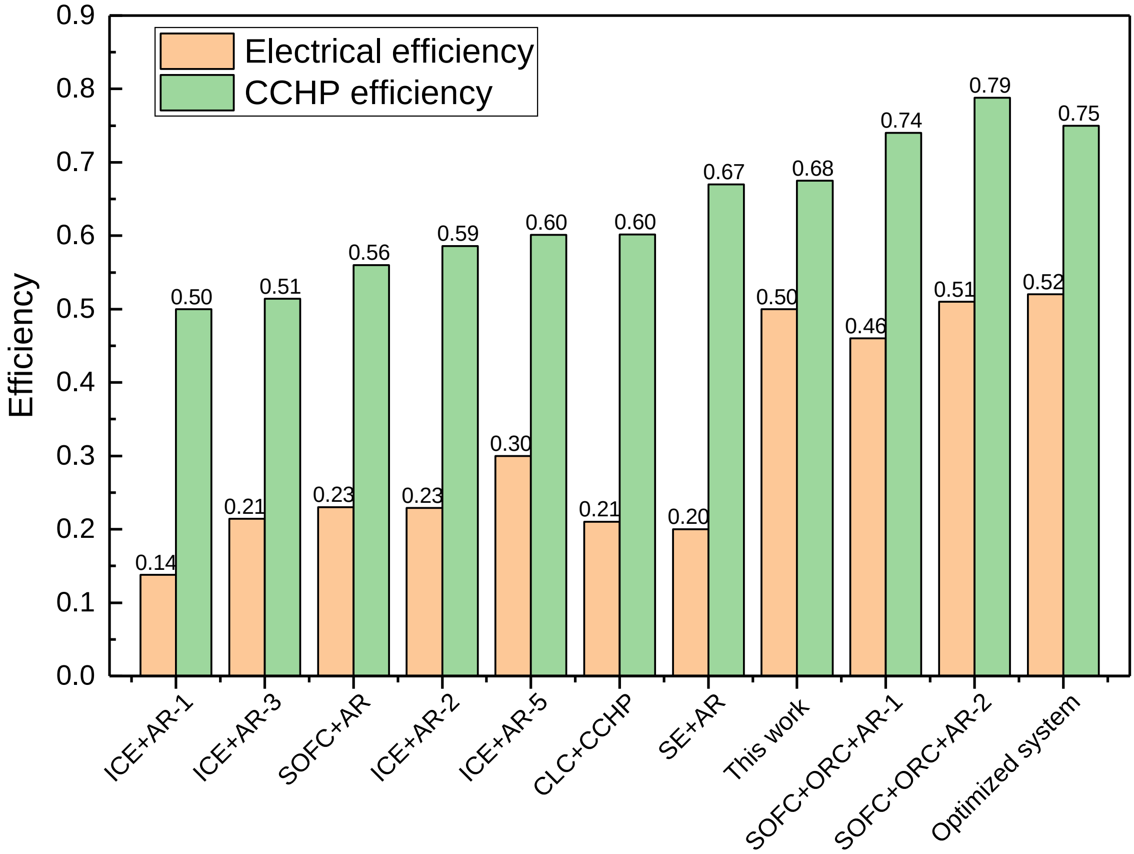

[ICE: Internal combustion engine; SE: Strling engine; AR: Absorption refrigeration; CLC: Chemical looping combustion; ORC: Organic Rankine cycle; GSHP: Ground source heat pump]

Fig. 13 The comparison of electrical and CCHP efficiency of various biomass based CCHP systems [39–47]

6 Conclusion

This work proposes a novel biomass-fueled SOFC-Engine combined cooling, heating and power poly-generation system for distributed scenarios. This novel CCHP system is modeled by Aspen Plus and investigated from first and second law of thermodynamic point view. Through the parametric analysis and multi-objective optimization, the tradeoff between efficiency and cost are conducted to achieve a high-efficiency and low-cost biomass-fueled CCHP system. In this work, the following conclusions can be drawn.

1) The performance comparison results show that the proposed novel poly-generation system is a kind of efficient energy conversion technology. When the inlet biomass is set as 500 kg/h, the system can generate 1000 kW of electrical power, 250 kW of heating power, and 99 kW of cooling power. Correspondingly, CCHP efficiency and net electrical efficiency are 67.5% and 50.0% without the optimization, respectively. Besides, the PESR is

calculated to be 41% through thermodynamic model, indicating the prior energy saving feature compared to the independent production system.

2) Through the parametric analysis, it is found that the increase of *S*/*B* ratio and fuel utilization factor μ as well as the decrease of air equivalent ratio *ER* contribute to improve the electrical efficiency. As *S*/*B* ratio increases from 0.5 to 1.0 the net electrical efficiency increases from 49.5% to 51.4% and as μ increases from 0.5 to 0.8, the net electrical efficiency increases from 45.7% to 50.0%.On the other hand, the biomass feedstock and the heat source temperature of absorption refrigeration significantly affects the CCHP efficiency by adjusting the output thermal or cooling power.
3) In the system, the biomass gasification and engine components account for the largest exergy destruction due to high-temperature chemical reaction, which is 511.7 kW and 182.9 kW, respectively. On the contrary, the exergy destruction of SOFC and absorption refrigeration subsystem is relatively low, which are 69.9 kW and 74.5 kW. Therefore, it is suggested to further optimize the thermodynamic performance of biomass gasification and engine units for this advanced CCHP system in future.
4) The multi-objective optimization shows that the CCHP system could reach the high efficiency of 75.0% and the low total annual cost of 410 k$ simultaneously. Besides, the net electrical efficiency can reach up to 52%, which is much higher than those of the previously reported CCHP hybrid systems based on thermal engine. Therefore, the proposed novel biomass-fueled CCHP system based on fuel cell is a clean, high-efficiency and low-cost poly-generation technology.

Acknowledgement

This work was financially sponsored by the National Key Research and Development Program of China (No.2018YFE0202000), the National Nature Science Foundation Project (No. 52050027), the China Education Association for International Exchange (No. 202006), the Natural Science Foundation Project of Shaanxi Province (No. 2020JM-014), and the Fundamental Research Funds for the Central Universities (No. xzd012020062).

Appendix A

Table A gives the cost equation of the components involved in the objective Function III TAC calculation process.

Table A The cost equations of components involved in the proposed CCHP system.

Component	Cost equation	Ref
Gasifier	$Z_{G} = 1600 \times (\dot{m}_{drybiomass})^{0.67}$	[13]
Reformer	$Z_{ER} = 130 \times \left(\frac{A_{ER}}{0.093}\right)^{0.78} + 3240 \times (V_{ER})^{0.4} + 2128 \times V_{ER}$	[23]
SOFC	$Z_{SOFC} = A \times N_{FC} \times (T_{FC} - 1907)$	[13]
SOFC auxiliary	$Z_{aux,SOFC} = 0.1 \times Z_{SOFC}$	[48]
Inverter	$Z_{inv} = 10^{5} \times \left(\frac{\dot{W}_{SOFC}}{500}\right)^{0.78}$	[13]
Air Blower	$Z_{AB} = 91562 \times \left(\frac{\dot{W}_{AB}}{455}\right)^{0.67}$	[49]
Water Pump	$Z_{WP} = 3 \times [442 \times (\dot{W}_{P})^{0.71} \times 1.41 f_{n}]$ $f_{n} = 1 + \frac{1-0.8}{1-\eta_{WP}}$	[13]
Engine	$Z_{HCCI}(\text{per Liter}) = 1.1 \times (9761.5 \times V_{engine}^{-0.9060})$	[49]
Heat exchanger	$Z_{HEX2} = 130 \times \left(\frac{A_{HEX}}{0.093}\right)^{0.78}$	[13]
Waste heat collector	$Z_{WHC} = 130 \times \left(\frac{A_{WHC}}{0.093}\right)^{0.78}$	[14]
Absorption refrigeration	$Z_{AR} = 158 \times \dot{W}_{AR}$	[50]

Appendix B

Table B gives the thermodynamic properties of each stream of the CCHP system in the simulation model.

Table B Thermodynamic properties of each streams of the hybrid system

Stream No.	P (bar)	T (°C)	NH_3 concentration (wt.%)	m (kg/h)	h (kJ/kg)	s (kJ/(kg·K)	$\dot{E}x^{ch}$ (kW)	$\dot{E}x^{ph}$ (kW)	$\dot{E}x$ (kW)
1	1	25.0	-	500	-3492.4	-	2422	0	2422
2	1	25.0	-	226.8	-0.2787	0.1511	0.003	0.281	0.283
3	2	98.0	-	226.8	73.69	0.0050	4.253	0.281	4.533
4	5	748.7	-	952.1	-5832.9	0.1733	249.1	1726	1975
5	5	748.7	-	32.34	10585.8	11.36	65.32	1052	1117
6	5	748.7	-	740.4	-8154.3	1.4964	163.3	597.6	760.9
7	5	765.2	-	740.4	-8154.5	1.5786	163.2	591.8	755.0
8	5	760.4	-	772.8	-7370.2	2.1863	225.1	1631	1856
9	2	800	-	3462.1	837.7	1.3145	477.8	4.283	482.1
10	5	972.6	-	4234.8	-1305.4	1.4451	986.8	576.8	1564
11	2	1067.2	-	4234.8	-1713.1	1.6315	1011	5.363	1017
12	1	25	-	3462.1	-0.2787	0.1511	0.041	4.283	4.324
13	2	98.0	-	3462.1	73.69	0.1733	64.92	4.283	69.20
14	2	601.4	-	4234.8	-2337.6	1.0609	473.5	5.363	478.9
15	1	25.0	-	300.0	-15972.1	-9.3240	0.016	3.469	3.485
16	5	25.0	-	300.0	-15971.6	-9.3240	0.055	3.469	3.524
17	5	300.0	-	300.0	-12904.4	-1.9629	75.83	3.469	79.30
18	2	427.7	-	4234.8	-2554.9	0.7841	313.3	5.362	318.7
19	2	250.0	-	4234.8	-2767.2	0.4351	183.9	5.363	189.3
20	15.56	97.5	0.3692	3600.0	-11344	-8.942	47.80	-	47.80
21	15.56	100.6	0.9612	313.8	-2989.7	-6.5229	34.65	-	34.65
22	15.56	114..6	0.3127	3286.2	-11931.7	-8.6203	57.15	-	57.15
23	15.56	30.0	0.9612	313.8	-4405.6	-10.894	22.90	-	22.90
24	2.5	-12.2	0.9612	313.8	-4405.6	-10.828	21.24	-	21.24
25	2.5	20.0	0.9612	313.8	-3272.5	-6.550	10.67	-	10.67
26	2.5	30.0	0.362	3600.0	-11665.8	-9.894	5.156	-	5.156
27	15.56	30.9	0.3692	3600.0	-11660.4	-9.882	7.038	-	7.038
28	2.5	42.0	0.3127	3286.2	-12278.3	-9.604	3.908	-	3.908
29	15.56	42.0	0.3127	3286.2	-12278.3	-9.609	5.384	-	5.384
30	2	108	-	4234.8	-2930.3	0.0718	117.4	5.363	122.8

References

[1] Naqvi SR, Jamshaid S, Naqvi M, Farooq W, Niazi MBK, Aman Z, et al. Potential of biomass for bioenergy in Pakistan based on present case and future perspectives. Renew Sustain Energy Rev 2018;81:1247–58. doi:10.1016/j.rser.2017.08.012.

[2] Wu N, Zhan X, Zhu X, Zhang Z, Lin J, Xie S, et al. Analysis of biomass polygeneration integrated energy system based on a mixed-integer nonlinear programming optimization method. J Clean Prod 2020;271:122761. doi:10.1016/j.jclepro.2020.122761.

[3] Islam MM, Hasanuzzaman M, Pandey AK, Rahim NA. Modern energy conversion technologies. Energy Sustain. Dev., Elsevier; 2020, p. 19–39. doi:10.1016/B978-0-12-814645-3.00002-X.

[4] Dong L, Liu H, Riffat S. Development of small-scale and micro-scale biomass-fuelled CHP systems – A literature review. Appl Therm Eng 2009;29:2119–26. doi:10.1016/j.applthermaleng.2008.12.004.

[5] Haseli Y. Maximum conversion efficiency of hydrogen fuel cells. Int J Hydrogen Energy 2018;43:9015–21. doi:10.1016/j.ijhydene.2018.03.076.

[6] Roushenas R, Razmi AR, Soltani M, Torabi M, Dusseault MB, Nathwani J. Thermo-environmental analysis of a novel cogeneration system based on solid oxide fuel cell (SOFC) and compressed air energy storage (CAES) coupled with turbocharger. Appl Therm Eng 2020;181:115978. doi:10.1016/j.applthermaleng.2020.115978.

[7] AlNouss A, McKay G, Al-Ansari T. A comparison of steam and oxygen fed biomass gasification through a techno-economic-environmental study. Energy Convers Manag 2020;208:112612. doi:10.1016/j.enconman.2020.112612.

[8] Radenahmad N, Azad AT, Saghir M, Taweekun J, Bakar MSA, Reza MS, et al. A review on biomass derived syngas for SOFC based combined heat and power application. Renew Sustain Energy Rev 2020;119:109560. doi:10.1016/j.rser.2019.109560.

[9] Yuksel YE, Ozturk M, Dincer I. Performance investigation of a combined biomass gasifier-SOFC plant for compressed hydrogen production. Int J Hydrogen Energy 2020;45:34679–94. doi:10.1016/j.ijhydene.2020.05.076.

[10] Gadsbøll RØ, Thomsen J, Bang-Møller C, Ahrenfeldt J, Henriksen UB. Solid oxide fuel cells powered by biomass gasification for high efficiency power generation. Energy 2017;131:198–206. doi:10.1016/j.energy.2017.05.044.

[11] Marcantonio V, Monarca D, Villarini M, Di Carlo A, Del Zotto L, Bocci E. Biomass Steam Gasification, High-Temperature Gas Cleaning, and SOFC Model: A Parametric Analysis. Energies 2020;13:5936. doi:10.3390/en13225936.

[12] Hosseinpour J, Chitsaz A, Liu L, Gao Y. Simulation of eco-friendly and affordable energy production via solid oxide fuel cell integrated with biomass gasification plant using various gasification agents. Renew Energy

2020;145:757–71. doi:10.1016/j.renene.2019.06.033.

[13] Habibollahzade A, Gholamian E, Houshfar E, Behzadi A. Multi-objective optimization of biomass-based solid oxide fuel cell integrated with Stirling engine and electrolyzer. Energy Convers Manag 2018;171:1116–33. doi:10.1016/j.enconman.2018.06.061.

[14] Wu Z, Zhu P, Yao J, Zhang S, Ren J, Yang F, et al. Combined biomass gasification, SOFC, IC engine, and waste heat recovery system for power and heat generation: Energy, exergy, exergoeconomic, environmental (4E) evaluations. Appl Energy 2020;279:115794. doi:10.1016/j.apenergy.2020.115794.

[15] Choi W, Kim J, Kim Y, Kim S, Oh S, Song HH. Experimental study of homogeneous charge compression ignition engine operation fuelled by emulated solid oxide fuel cell anode off-gas. Appl Energy 2018;229:42–62. doi:10.1016/j.apenergy.2018.07.086.

[16] Wu Z, Tan P, Zhu P, Cai W, Chen B, Yang F, et al. Performance analysis of a novel SOFC-HCCI engine hybrid system coupled with metal hydride reactor for H2 addition by waste heat recovery. Energy Convers Manag 2019;191:119–31. doi:10.1016/j.enconman.2019.04.016.

[17] Mehr AS, MosayebNezhad M, Lanzini A, Yari M, Mahmoudi SMS, Santarelli M. Thermodynamic assessment of a novel SOFC based CCHP system in a wastewater treatment plant. Energy 2018;150:299–309. doi:10.1016/j.energy.2018.02.102.

[18] Zhao H, Hou Q. Thermodynamic performance study of the MR SOFC-HAT-CCHP system. Int J Hydrogen Energy 2019;44:4332–49. doi:10.1016/j.ijhydene.2018.12.129.

[19] Mehrpooya M, Sadeghzadeh M, Rahimi A, Pouriman M. Technical performance analysis of a combined cooling heating and power (CCHP) system based on solid oxide fuel cell (SOFC) technology – A building application. Energy Convers Manag 2019;198:111767. doi:10.1016/j.enconman.2019.06.078.

[20] Jing R, Wang M, Wang W, Brandon N, Li N, Chen J, et al. Economic and environmental multi-optimal design and dispatch of solid oxide fuel cell based CCHP system. Energy Convers Manag 2017;154:365–79. doi:10.1016/j.enconman.2017.11.035.

[21] Al Moussawi H, Fardoun F, Louahlia H. 4-E based optimal management of a SOFC-CCHP system model for residential applications. Energy Convers Manag 2017;151:607–29. doi:10.1016/j.enconman.2017.09.020.

[22] Bahng G, Jang D, Kim Y, Shin M. A new technology to overcome the limits of HCCI engine through fuel modification. Appl Therm Eng 2016;98:810–5. doi:10.1016/j.applthermaleng.2015.12.076.

[23] Sarabchi N, Mahmoudi SMS, Yari M, Farzi A. Exergoeconomic analysis and optimization of a novel hybrid cogeneration system: High-temperature proton exchange membrane fuel cell/Kalina cycle, driven by solar energy.

Energy Convers Manag 2019;190:14–33. doi:10.1016/j.enconman.2019.03.037.

[24] Wang Y, Wehrle L, Banerjee A, Shi Y, Deutschmann O. Analysis of a biogas-fed SOFC CHP system based on multi-scale hierarchical modeling. Renew Energy 2021;163:78–87. doi:10.1016/j.renene.2020.08.091.

[25] Xiao J, Shen L, Zhang Y, Gu J. Integrated Analysis of Energy, Economic, and Environmental Performance of Biomethanol from Rice Straw in China. Ind Eng Chem Res 2009;48:9999–10007. doi:10.1021/ie900680d.

[26] Wu Z, Zhu P, Yao J, Tan P, Xu H, Chen B, et al. Dynamic modeling and operation strategy of natural gas fueled SOFC-Engine hybrid power system with hydrogen addition by metal hydride for vehicle applications. ETransportation 2020;5:100074. doi:10.1016/j.etran.2020.100074.

[27] Yang S, Wang Y, Gao J, Zhang Z, Liu Z, Olabi AG. Performance Analysis of a Novel Cascade Absorption Refrigeration for Low-Grade Waste Heat Recovery. ACS Sustain Chem Eng 2018;6:8350–63. doi:10.1021/acssuschemeng.8b00397.

[28] Valero, Alicia, Valero A. The Exergy Calculator. Online Tool Available Exergoecology Portal 2018. http://www.exergoecology.com/.

[29] Zhang X, Li H, Liu L, Bai C, Wang S, Song Q, et al. Exergetic and exergoeconomic assessment of a novel CHP system integrating biomass partial gasification with ground source heat pump. Energy Convers Manag 2018;156:666–79. doi:10.1016/j.enconman.2017.11.075.

[30] Jiang R, Han W, Qin FGF, Sui J, Yin H, Yang M, et al. Thermodynamic model development, experimental validation and performance analysis of a MW CCHP system integrated with dehumidification system. Energy Convers Manag 2018;158:176–85. doi:10.1016/j.enconman.2017.12.060.

[31] Arsalis A. Thermoeconomic modeling and parametric study of hybrid SOFC–gas turbine–steam turbine power plants ranging from 1.5 to 10MWe. J Power Sources 2008;181:313–26. doi:10.1016/j.jpowsour.2007.11.104.

[32] Wu Z, Zhu P, Yao J, Tan P, Xu H, Chen B, et al. Thermo-economic modeling and analysis of an NG-fueled SOFC-WGS-TSA-PEMFC hybrid energy conversion system for stationary electricity power generation. Energy 2020;192:116613. doi:10.1016/j.energy.2019.116613.

[33] Jing R, Zhu X, Zhu Z, Wang W, Meng C, Shah N, et al. A multi-objective optimization and multi-criteria evaluation integrated framework for distributed energy system optimal planning. Energy Convers Manag 2018;166:445–62. doi:10.1016/j.enconman.2018.04.054.

[34] Fremaux S, Beheshti S-M, Ghassemi H, Shahsavan-Markadeh R. An experimental study on hydrogen-rich gas production via steam gasification of biomass in a research-scale fluidized bed. Energy Convers Manag 2015;91:427–32. doi:10.1016/j.enconman.2014.12.048.

[35] Pala LPR, Wang Q, Kolb G, Hessel V. Steam gasification of biomass with subsequent syngas adjustment using shift reaction for syngas production: An Aspen Plus model. Renew Energy 2017;101:484–92. doi:10.1016/j.renene.2016.08.069.

[36] ZHAO F, VIRKAR A. Dependence of polarization in anode-supported solid oxide fuel cells on various cell parameters. J Power Sources 2005;141:79–95. doi:10.1016/j.jpowsour.2004.08.057.

[37] Herold KE, Radermacher R, Klein SA. Absorption Chillers and Heat Pumps. Second Edi. CRC Press; 2016.

[38] Somers C, Mortazavi A, Hwang Y, Radermacher R, Rodgers P, Al-Hashimi S. Modeling water/lithium bromide absorption chillers in ASPEN Plus. Appl Energy 2011;88:4197–205. doi:10.1016/j.apenergy.2011.05.018.

[39] Coronado CR, Yoshioka JT, Silveira JL. Electricity, hot water and cold water production from biomass. Energetic and economical analysis of the compact system of cogeneration run with woodgas from a small downdraft gasifier. Renew Energy 2011;36:1861–8. doi:10.1016/j.renene.2010.11.021.

[40] Zhang X, Liu X, Sun X, Jiang C, Li H, Song Q, et al. Thermodynamic and economic assessment of a novel CCHP integrated system taking biomass, natural gas and geothermal energy as co-feeds. Energy Convers Manag 2018;172:105–18. doi:10.1016/j.enconman.2018.07.002.

[41] Wang J-J, Yang K, Xu Z-L, Fu C. Energy and exergy analyses of an integrated CCHP system with biomass air gasification. Appl Energy 2015;142:317–27. doi:10.1016/j.apenergy.2014.12.085.

[42] Huang Y, Wang YD, Rezvani S, McIlveen-Wright DR, Anderson M, Hewitt NJ. Biomass fuelled trigeneration system in selected buildings. Energy Convers Manag 2011;52:2448–54. doi:10.1016/j.enconman.2010.12.053.

[43] Ozcan H, Dincer I. Performance evaluation of an SOFC based trigeneration system using various gaseous fuels from biomass gasification. Int J Hydrogen Energy 2015;40:7798–807. doi:10.1016/j.ijhydene.2014.11.109.

[44] Al-Sulaiman FA, Dincer I, Hamdullahpur F. Energy analysis of a trigeneration plant based on solid oxide fuel cell and organic Rankine cycle. Int J Hydrogen Energy 2010;35:5104–13. doi:10.1016/j.ijhydene.2009.09.047.

[45] Palomba V, Prestipino M, Galvagno A. Tri-generation for industrial applications: Development of a simulation model for a gasification-SOFC based system. Int J Hydrogen Energy 2017;42:27866–83. doi:10.1016/j.ijhydene.2017.06.206.

[46] Huang Y, Wang YD, Chen H, Zhang X, Mondol J, Shah N, et al. Performance analysis of biofuel fired trigeneration systems with energy storage for remote households. Appl Energy 2017;186:530–8. doi:10.1016/j.apenergy.2016.03.028.

[47] Fan J, Hong H, Zhu L, Jiang Q, Jin H. Thermodynamic and environmental evaluation of biomass and coal co-fuelled gasification chemical looping combustion with CO 2 capture for combined cooling, heating and power

production. Appl Energy 2017;195:861–76. doi:10.1016/j.apenergy.2017.03.093.

[48] Chen Y, Wang M, Liso V, Samsatli S, Samsatli NJ, Jing R, et al. Parametric analysis and optimization for exergoeconomic performance of a combined system based on solid oxide fuel cell-gas turbine and supercritical carbon dioxide Brayton cycle. Energy Convers Manag 2019;186:66–81. doi:10.1016/j.enconman.2019.02.036.

[49] Lee YD, Ahn KY, Morosuk T, Tsatsaronis G. Exergetic and exergoeconomic evaluation of an SOFC-Engine hybrid power generation system. Energy 2018;145:810–22. doi:10.1016/j.energy.2017.12.102.

[50] Hou Q, Zhao H, Yang X. Economic performance study of the integrated MR-SOFC-CCHP system. Energy 2019;166:236–45. doi:10.1016/j.energy.2018.10.072.

CRediT authorship contribution statement

Pengfei Zhu: Writing-original draft, Software, Validation, Conceptualization, Methodology.

Jing Yao: Data curation, Formal analysis.

Leilei Guo: Validation

Min Dai: Software, Formal analysis.

Jianwei Ren: Supervision, Resources.

Sandra Kurko: Supervision

Zhen Wu: Writing-Review & Editing, Supervision, Funding acquisition.

Fusheng Yang: Supervision, Resources

Zaoxiao Zhang: Supervision, Resources.

Declaration of interests

☒ The authors declare that they have no known competing financial interests or personal relationships that could have appeared to influence the work reported in this paper.

☐The authors declare the following financial interests/personal relationships which may be considered as potential competing interests: